nature communications

Article

https://doi.org/10.1038/s41467-024-51078-2

Adipose tissue macrophage infiltration and hepatocyte stress increase GDF-15 throughout development of obesity to MASH

Received: 19 October 2023

Accepted: 29 July 2024

Published online: 21 August 2024

Check for updates

Laurent L'homme[1], Benan Pelin Sermikli[1], Joel T. Haas[1], Sébastien Fleury[1], Sandrine Quemener[1], Valentine Guinot[1], Emelie Barreby[2], Nathalie Esser[3,4], Robert Caiazzo[5], Hélène Verkindt[5], Benjamin Legendre[5], Violeta Raverdy[5], Lydie Cheval[6,7], Nicolas Paquot[3,4], Jacques Piette[8], Sylvie Legrand-Poels[3], Myriam Aouadi[2], François Pattou[5], Bart Staels[1] & David Dombrowicz[1]

Plasma growth differentiation factor-15 (GDF-15) levels increase with obesity and metabolic dysfunction-associated steatotic liver disease (MASLD) but the underlying mechanism remains poorly defined. Using male mouse models of obesity and MASLD, and biopsies from carefully-characterized patients regarding obesity, type 2 diabetes (T2D) and MASLD status, we identify adipose tissue (AT) as the key source of GDF-15 at onset of obesity and T2D, followed by liver during the progression towards metabolic dysfunction-associated steatohepatitis (MASH). Obesity and T2D increase *GDF15* expression in AT through the accumulation of macrophages, which are the main immune cells expressing *GDF15*. Inactivation of *Gdf15* in macrophages reduces plasma GDF-15 concentrations and exacerbates obesity in mice. During MASH development, *Gdf15* expression additionally increases in hepatocytes through stress-induced TFEB and DDIT3 signaling. Together, these results demonstrate a dual contribution of AT and liver to GDF-15 production in metabolic diseases and identify potential therapeutic targets to raise endogenous GDF-15 levels.

Obesity is a worldwide public health issue and a major risk factor for the development of type 2 diabetes (T2D) and metabolic dysfunction-associated steatotic liver disease (MASLD). Obesity-related expansion of adipose tissue (AT) is associated with infiltration and activation of immune cells, such as macrophages, leading to a state of chronic and low-grade inflammation[1]. Both AT expansion and inflammation play major roles in the pathogenesis of T2D through several mechanisms including the release of cytokines directly interfering with the insulin signaling pathway[2]. Together, obesity and insulin resistance favor excessive lipid accumulation in the liver and contribute to the

[1]Univ. Lille, INSERM, CHU Lille, Institut Pasteur de Lille, U1011-EGID, Lille, France. [2]Center for Infectious Medicine (CIM), Department of Medicine Huddinge, Karolinska Institutet, Karolinska University Hospital, Stockholm, Sweden. [3]Laboratory of Immunometabolism and Nutrition, GIGA-I3, University of Liège, Liège, Belgium. [4]Division of Diabetes, Nutrition and Metabolic Disorders, Department of Medicine, CHU Liège, Liège, Belgium. [5]Univ. Lille, INSERM, CHU Lille, Institut Pasteur de Lille, U1190-EGID (Translational research in Diabetes), Lille, France. [6]Centre de Recherche des Cordeliers, INSERM, Sorbonne Université, Université Paris Cité, Laboratoire de Physiologie Rénale et Tubulopathies, Paris, France. [7]CNRS EMR 8228—Unité Métabolisme et Physiologie Rénale, Paris, France. [8]Laboratory of Virology and Immunology, GIGA-Signal Transduction, University of Liège, Liège, Belgium. e-mail: laurent.l-homme@inserm.fr; david.dombrowicz@pasteur-lille.fr

development of MASLD[3,4]. MASLD encompasses a spectrum of steatotic liver conditions in patients presenting at least one cardiometabolic risk factor. It ranges from simple steatosis (metabolic dysfunction-associated steatotic liver, MASL) to metabolic dysfunction-associated steatohepatitis (MASH) with steatosis, inflammatory infiltrates and hepatocyte ballooning as disease-defining features. The progression from MASL to MASH is not fully understood, but involves several cellular processes such as inflammation, lysosomal/autophagy dysfunction, mitochondrial dysfunction, endoplasmic reticulum (ER) stress and integrated stress response (ISR), likely resulting from hepatic lipotoxicity[3,4]. The metabolic triad of obesity, T2D and MASLD is common and challenges the separate study of these entities.

Growth differentiation factor-15 (GDF-15) is a cytokine belonging to the transforming growth factor-beta (TGF-β) superfamily. *GDF15* is widely expressed with the highest expression levels observed in placenta, prostate, kidney, pancreas, liver and AT[5–7]. GDF-15 binds to the GDNF family receptor alpha-like (GFRAL) which induces cellular signaling through its co-receptor Ret[8–10]. Despite the wide expression of Ret, GFRAL expression is restricted to the neurons of two brainstem regions, the area postrema and the nucleus of the solitary tract[8–10], both involved in the regulation of appetite. Activation of the GDF-15/GFRAL pathway negatively regulates food intake[8–11] and represents therefore an attractive target for the development of new therapies against obesity[12]. Beyond its anorectic properties, it was also proposed that GDF-15 increases energy expenditure[11,13,14], fatty acid oxidation[8,14] and has anti-inflammatory properties[15,16]. In line with these protective roles, both *Gdf15*- and *Gfral*-deficient mice develop more severe obesity, insulin resistance and MASLD-like conditions[8,9,17,18], while *GDF15* overexpression or injection of rGDF-15 prevent these conditions[8,9,11,13,14,19,20]. Although it provides a protection against weight gain, plasma GDF-15 levels increase with obesity and its complications[21–24].

Why and how GDF-15 levels increase in obesity remains however controversial and not fully understood. Indeed, an earlier study reported that *GDF15* expression increases in AT of patients with obesity[25], while another did not observe such obesity-related changes[21]. Similarly, increased liver *GDF15* expression was reported in mouse models of long-term obesity[19,26], but not in short-term models[27]. Importantly, the expression of *GDF15* increases in livers of patients with MASLD[16], a common comorbidity of obesity, raising the possibility that liver *GDF15* expression is regulated by MASLD and not obesity. Furthermore, the molecular mechanism underlying the elevation of GDF-15 levels in obesity remains largely unknown, despite the fact that GDF-15 is a promising therapeutic target for obesity[12] and that a better understanding of GDF-15 regulation is critical to develop new therapies to raise endogenous GDF-15 production.

Thus, we performed a detailed study covering the spectrum of obesity and its major complications to identify the tissular and cellular source of GDF-15 over disease progression and determine the molecular mechanisms regulating its expression. By using a large human cohort extensively characterized for obesity, T2D and MASLD status, and several experimental mouse models of obesity, insulin resistance and MASLD-like conditions, we identify a progressive increase of plasma GDF-15 levels during the sequential development of obesity, T2D and MASLD. The production of GDF-15 first increases in AT at the onset of obesity and T2D and subsequently in liver during MASLD progression. Macrophages express high levels of *GDF15* and their accumulation in AT accounts for GDF-15 elevation in obesity and T2D. The inactivation of *Gdf15* in macrophages reduces plasma GDF-15 concentrations and exacerbates diet-induced obesity in mice. The development of liver complications, especially the progression from steatosis to MASH, further enhances GDF-15 production by hepatocytes through the activation of TFEB and DDIT3 signaling pathways related to MASLD-associated cellular stress.

Results

AT is the main source of GDF-15 in obesity and T2D

To identify the source of GDF-15 in obesity, we fed mice a 60% high-fat diet (HFD) for 12 weeks (Supplementary Fig. 1A–C). As expected, HFD-fed mice displayed higher plasma GDF-15 concentrations compared to mice on chow diet (Fig. 1A). *Gdf15* expression was induced in epiAT and, to a lesser extent, in liver from HFD-fed mice compared to control mice (Fig. 1B). In HFD-fed mice, *Gdf15* was predominantly expressed in liver, epididymal AT (epiAT) and kidney, while muscle, intestine, spleen, lung and inguinal AT (ingAT) showed low expression levels (Supplementary Fig. 1D). Plasma GDF-15 concentrations correlated positively and significantly with *Gdf15* expression in epiAT, but not in liver (Fig. 1C), suggesting that epiAT accounts for most of the increased plasma GDF-15 concentrations in HFD-induced obesity. The expression of the GDF-15 receptor, *Gfral*, was virtually not detected and not regulated by obesity in peripheral tissues (Supplementary Fig. 1E).

In patients with obesity, we also observed a higher *GDF15* expression in visceral AT (VAT) and a trend toward higher expression in subcutaneous AT (SAT) compared to individuals without obesity (Fig. 1D). However, *GDF15* expression was not significantly upregulated in the liver of patients with obesity despite a high expression in some individuals (Fig. 1E). Unlike in mice, *GFRAL* expression was lowly detected in SAT of >50% of individuals (Supplementary Fig. 1F, G). However, obesity had no impact on its detection or its expression. Obesity-related clinical parameters (weight, BMI and waist circumference) all positively correlated with *GDF15* expression in VAT (Fig. 1F). *GDF15* expression in VAT also positively associated with glycemic parameters, but not with blood lipids, age, sex or height. Associations between *GDF15* expression in VAT and obesity or glycemic parameters remained significant after adjustments for age and sex (Supplementary Table 3). Similar results were obtained in VAT and SAT from an independent cohort of patients with obesity (Supplementary Fig. 1H, I). Stratification of patients with obesity according to T2D status revealed a higher *GDF15* expression in VAT of patients with obesity and T2D (Fig. 1G). Likewise, significantly higher expression was observed in SAT from patients with obesity and T2D (Fig. 1H), suggesting that SAT may also contribute to GDF-15 production in obesity with T2D. Importantly, there were no differences in obesity parameters such as BMI or waist circumference between patients with and without T2D (Supplementary Table 1), emphasizing an additive contribution of T2D in a context of obesity. Moreover, associations between *GDF15* expression in VAT and glycemic parameters remained significant after adjustment for obesity (Supplementary Table 3). Unlike VAT and SAT, *GDF15* expression in liver was not induced by T2D in patients with obesity (Fig. 1I). Altogether, these results show that visceral fat, and to a lesser extent subcutaneous fat in humans, display increased expression of *GDF15* with obesity. Moreover, the presence of T2D in patients with obesity further increases *GDF15* expression in AT.

Liver is an additional source of GDF-15 during MASLD progression

Although obesity and T2D do not result in a higher expression of *GDF15* in human livers (Fig. 1E, I), a modest increase was observed in livers of mice on HFD feeding (Fig. 1B). As the HFD-induced obesity model affects liver function and broadly reproduces human MASL (Supplementary Fig. 2A), we next examined whether *GDF15* expression is associated with pathophysiological liver condition in patients covering MASLD spectrum (Supplementary Table 2). We observed a strong correlation between hepatic *GDF15* expression and clinical liver parameters including steatosis, inflammation, ballooning, NAS, fibrosis and plasma transaminases activity (Fig. 2A). Associations between *GDF15* expression in liver and inflammation, ballooning, NAS and fibrosis remained highly significant after adjustment for age, sex, obesity and T2D (Supplementary Table 4). Furthermore, classification of patients with obesity according to MASLD status revealed a significantly higher

https://doi.org/10.1038/s41467-024-51078-2

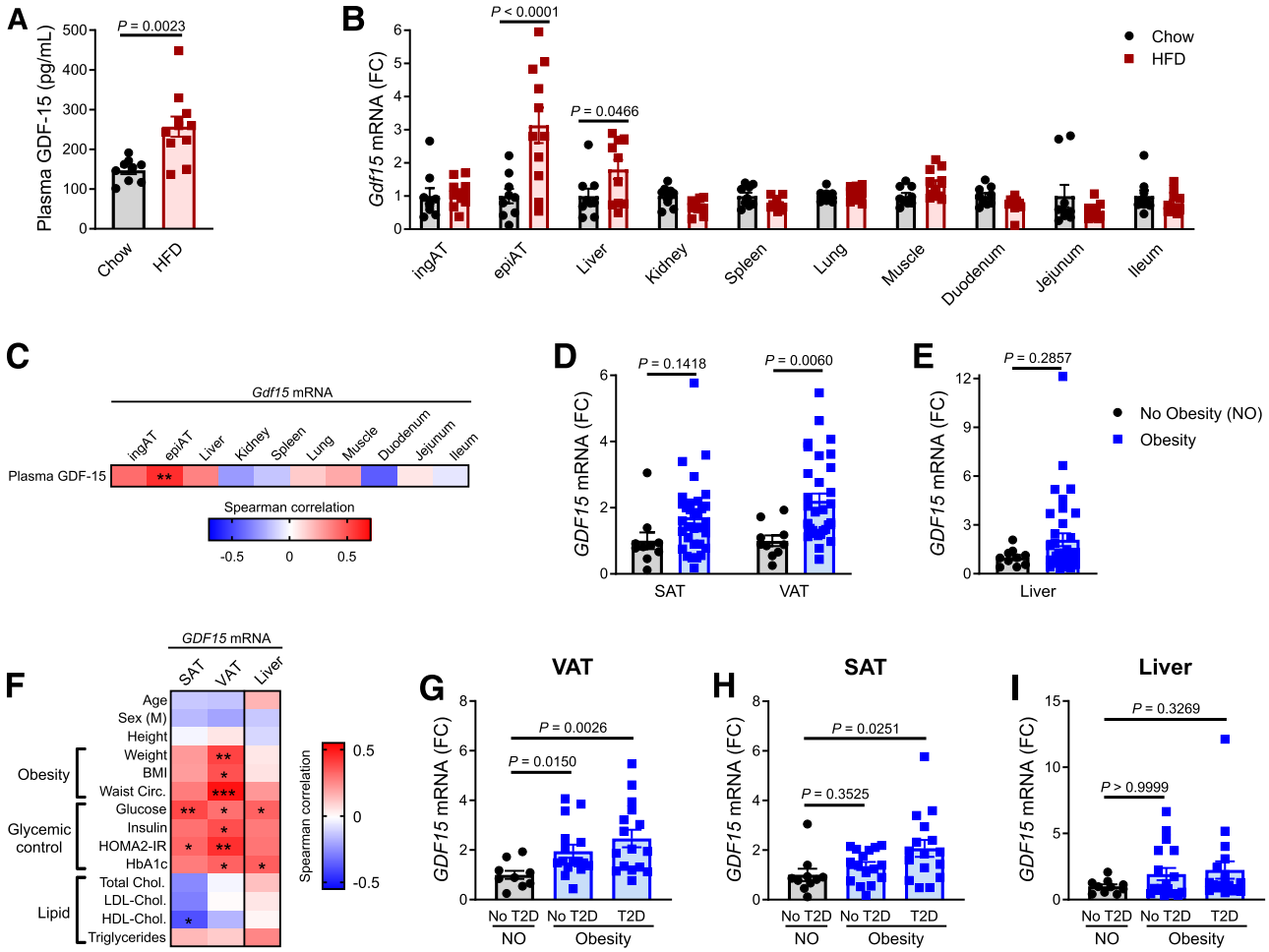

Fig. 1 | GDF-15 is produced by AT in obesity and T2D. A–C Mice were fed a chow ($n = 9$) or a HFD ($n = 11$) for 12 weeks. **A** Plasma GDF-15 concentrations. **B** *Gdf15* mRNA expression levels in tissues. **C** Correlation between plasma GDF-15 concentrations and *Gdf15* mRNA expression levels. **D–I** Analysis of paired subcutaneous AT (SAT) and visceral AT (VAT) ($n = 42$) or liver ($n = 46$) biopsies from patients. **D**, **E** *GDF15* mRNA expression levels according to obesity status. **F** Correlation between *GDF15* mRNA expression levels and clinical parameters. **G–I** *GDF15* mRNA expression levels according to T2D status. Data are shown as mean ± SEM. *P* values calculated by two-tailed Mann–Whitney test (**A**, **E**), 2-way ANOVA followed by Sidak's multiple comparisons test (**B**, **D**), two-tailed Spearman correlation (**C**, **F**) or Kruskal–Wallis test followed by Dunn's multiple comparisons test (**G–I**). $^{*}P < 0.05$; $^{**}P < 0.01$; $^{***}P < 0.001$; FC fold change. Source data are provided as a Source Data file.

expression of *GDF15* in the liver of patients with MASH (Fig. 2B). Importantly, using liver microarray data from 840 individuals with obesity and histologically assessed MASLD status, we confirmed the high *GDF15* expression level in MASH patients and observed a less pronounced, but significant, increase in MASL patients compared to individuals without MASLD (Fig. 2C). Moreover, the expression of *GDF15* in liver strongly associated with clinical liver parameters, but only modestly with obesity or glycemic parameters (Fig. 2D). These results show that *GDF15* expression in liver follows the evolution of MASLD rather than obesity or T2D and suggest that MASH is an additional factor potentially contributing to plasma GDF-15 levels on top of obesity and T2D.

To confirm this hypothesis, we measured plasma GDF-15 concentrations in patients matched for obesity and T2D in order to determine the progressive impact of obesity, T2D and MASH (Fig. 2E and Supplementary Table 5). Plasma GDF-15 concentrations were higher in patients with obesity alone and even more in patients with obesity and T2D compared to patients without obesity (Fig. 2E). Patients with MASH further displayed higher plasma GDF-15 concentrations compared to patients without MASLD, supporting that MASH increases plasma GDF-15 levels in addition to obesity and T2D (Fig. 2E).

As we observed that patients with obesity and MASL already display a higher expression of *GDF15* in liver compared to subjects without MASLD (Fig. 2C), we further refined patient stratification according to the most frequent path of disease progression in order to better delineate the impact of MASLD on *GDF15* expression. We found a nearly significant difference in hepatic *GDF15* expression in patients with obesity and liver steatosis alone compared to patients with obesity but without steatosis, inflammation nor ballooning (Fig. 2F). Hepatic *GDF15* expression was higher in patients with obesity, steatosis and lobular inflammation with a major elevation occurring in patients who additionally displayed hepatocyte ballooning and met all MASH criteria (Fig. 2F). In line with this observation, receiver operating characteristic (ROC) curve analysis showed that liver *GDF15* expression better predicted the presence of MASH than MASL (Fig. 2G). Among the histological diagnosis criteria of MASH, the area under the curve (AUC) of the ROC curve was the highest for the presence of ballooning, but lower for inflammation or steatosis (Fig. 2H). Altogether, these results show that hepatic *GDF15* expression increases with MASLD progression with a major elevation observed at a later stage with ballooning development and the emergence of MASH.

To further delineate the specific contribution of MASH on GDF-15 production by liver, we used experimental mouse models of

https://doi.org/10.1038/s41467-024-51078-2

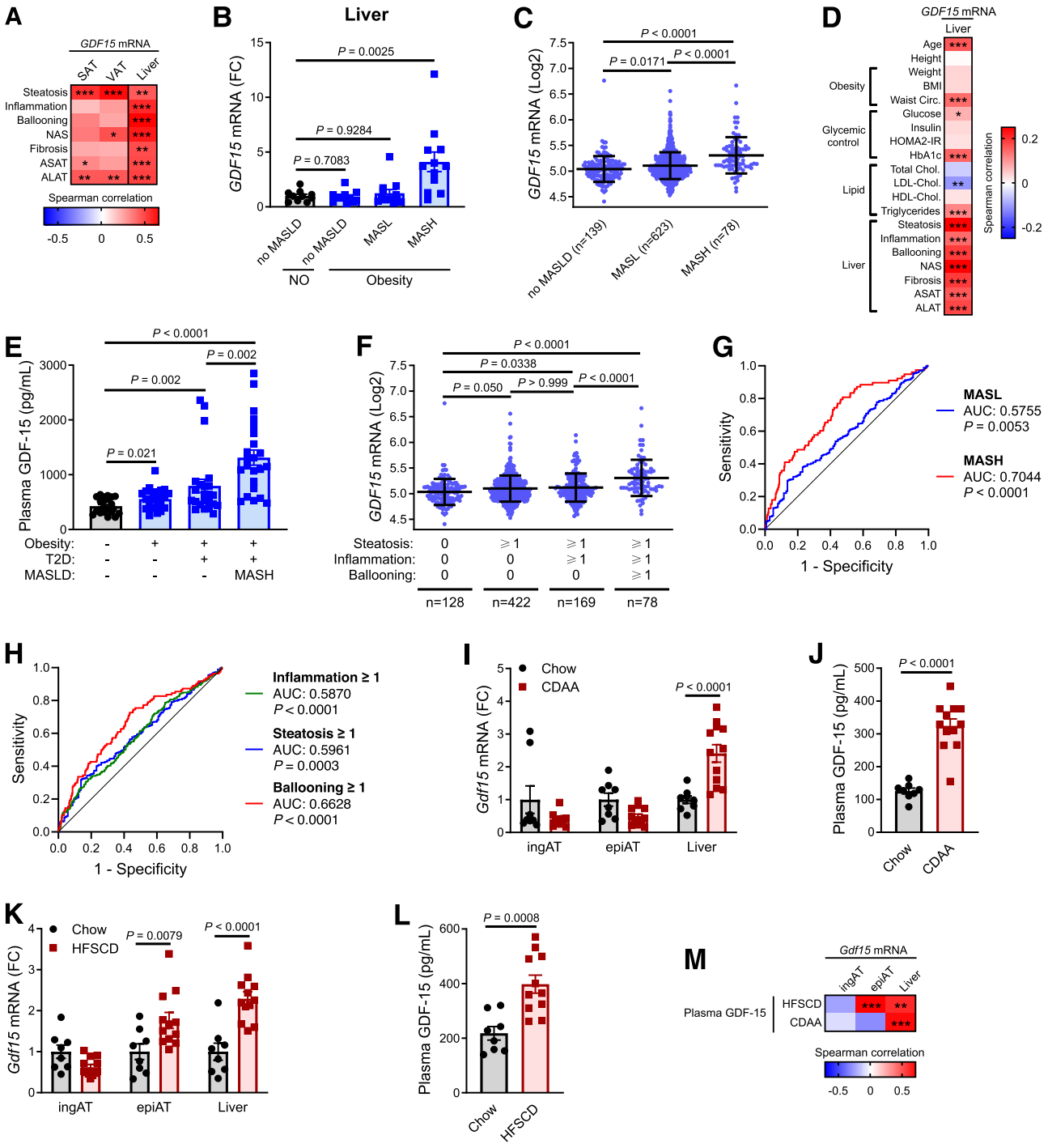

Fig. 2 | GDF-15 is produced by liver in MASH. A Correlation between liver parameters and *GDF15* mRNA expression levels in paired SAT and VAT ($n = 42$) or liver ($n = 46$). **B** *GDF15* mRNA expression levels in liver according to MASLD status ($n = 46$). **C** *GDF15* mRNA expression levels in liver of patients with obesity measured by microarray according to MASLD status ($n = 840$). **D** Correlation between clinical parameters and *GDF15* mRNA expression levels in liver of patients with obesity measured by microarray ($n = 840$). **E** Plasma GDF-15 concentrations ($n = 23$/group). **F** *GDF15* mRNA expression levels in liver measured by microarray according to conventional disease progression ($n = 797$). **G** ROC curve of *GDF15* mRNA expression levels in liver measured by microarray to predict MASL (vs no MASLD) or MASH (vs no MASLD & MASL). **H** ROC curve of *GDF15* mRNA expression levels in liver measured by microarray to predict steatosis, inflammation or ballooning (≥1 vs 0). **I, J** Mice were fed a chow ($n = 8$) or a CDAA diet ($n = 12$) for 8 weeks. **I** *Gdf15* mRNA expression levels in tissues. **J** Plasma GDF-15 concentrations. **K, L** Mice were fed a chow ($n = 8$) or a HFSCD ($n = 12$) for 24 weeks. **K** *Gdf15* mRNA expression levels in tissues. **L** Plasma GDF-15 concentrations. **M** Correlation between plasma GDF-15 concentrations and *Gdf15* mRNA expression levels in tissues according to diet ($n = 20$/diet). Data are shown as mean ± SEM or SD (**C**, **F**). *P* values calculated by two-tailed Spearman correlation (**A**, **D**, **M**), Kruskal–Wallis test followed by two-stage linear step-up procedure of Benjamini, Krieger and Yekutieli (**B**, **E**), Kruskal–Wallis test followed by Dunn's multiple comparisons test (**C**, **F**), ROC analysis (**G**, **H**), 2-way ANOVA followed by Sidak's multiple comparisons test (**I**, **K**) or two-tailed Mann–Whitney test (**J**, **L**). $^{*}P < 0.05$; $^{**}P < 0.01$; $^{***}P < 0.001$; FC fold change, AUC area under the curve. Source data are provided as a Source Data file.

steatohepatitis, with or without concomitant obesity and insulin resistance. First, we fed mice a choline-deficient, L-amino acid-defined (CDAA) diet for 8 weeks which drives steatohepatitis without body weight gain and hyperglycemia[28] (Supplementary Fig. 2A–D). CDAA diet feeding increased *Gdf15* expression in liver, but not in AT (Fig. 2I). Moreover, the plasma GDF-15 concentration was higher in mice fed the CDAA diet than in control mice (Fig. 2J), confirming that steatohepatitis intrinsically increases *Gdf15* expression in the liver and plasma GDF-15 levels independently of obesity and insulin resistance. Second, in a diet model more closely related to human MASH, where mice are fed a high-fat high-sucrose diet enriched in cholesterol (HFSCD) for 24 weeks and develop obesity, hyperglycemia and MASH-like disease (Supplementary Fig. 2A, 2E–G), *Gdf15* expression was also higher in liver (Fig. 2K). Similar to HFD, the HFSCD also increased epiAT *Gdf15* expression and plasma concentrations (Fig. 2K, L). While plasma GDF-15 concentrations only correlated with liver *Gdf15* expression in the CDAA diet model, it correlated with both liver and epiAT *Gdf15* expression in the HFSCD model (Fig. 2M), in line with the steatohepatitis and obesity that develop in this model. Taken together these results suggest that in both humans and mice, obesity and T2D initially contribute to plasma GDF-15 levels by increasing its expression in AT while at a later stage, the development of MASLD, and particularly MASH, plays an additional role by increasing hepatic GDF-15 production.

Macrophages are the main source of GDF-15 in obese AT

We next determined the cellular source of GDF-15 in AT and liver. Immunohistochemistry analysis of epiAT from HFD-fed mice revealed GDF-15 staining in non-parenchymal cells (Fig. 3A) and particularly within inflammatory infiltrates and crown-like structures, both known to be mostly composed of macrophages[29,30]. To confirm that adipose tissue macrophages (ATMs) express *Gdf15*, we fractionated epiAT from HFD-fed mice into adipocytes and the stromal vascular fraction (SVF), which was further sorted by flow cytometry into four fractions: (i) ATMs ($CD45^+$ Lin^- $F4/80^+$ $CD64^+$), (ii) non-ATM immune cells ($CD45^+$ Lin^+ and $CD45^+$ Lin^- $F4/80^-$ $CD64^-$), (iii) adipose-derived stem cells (ADSCs) ($CD45^-$ $CD34^+$ $CD31^-$) and (iv) $CD45^-$ non-ADSCs ($CD45^-$ $CD34^{int/-}$ $CD31^{+/-}$) (Supplementary Fig. 3A). Corroborating the immunohistochemistry analysis, ATMs expressed the highest level of *Gdf15* among the five fractions analyzed (Fig. 3B). In available single cell RNA-sequencing data[31], we also observed that *Gdf15* was mainly detected in macrophages among epiAT $CD45^+$ cells from HFD-fed mice (Supplementary Fig. 3B, C). *Gdf15* expression was lower in resident macrophages compared to lipid-associated macrophages (LAMs) or cycling macrophages (Supplementary Fig. 3D–F), suggesting a certain heterogeneity in *Gdf15* expression among ATMs. In naive mice, the expression of *Gdf15* was also heterogeneous according to tissue origin, with epiAT macrophages expressing the highest levels (Fig. 3C). Moreover, the high expression of *Gdf15* was limited to macrophages among immune cells (Fig. 3C). Similar results were obtained by reanalyzing *Gdf15* expression in the publicly available ImmGen mouse database (Supplementary Fig. 3G).

Importantly, the expression of macrophage markers, but not lymphocyte markers, was positively associated with *Gdf15* expression in epiAT and plasma GDF-15 concentrations (Fig. 3D). Moreover, among the various immune cell populations identified by flow cytometry within mouse AT (Supplementary Fig. 3H–J), only the macrophage content in epiAT positively and consistently correlated with both *Gdf15* expression and plasma GDF-15 concentrations (Fig. 3E). Together these results show that ATMs express high levels of *Gdf15* and that their accumulation in epiAT is strongly associated with tissue expression and plasma level of GDF-15, suggesting that ATMs are a major source of GDF-15 in epiAT from obese mice.

Macrophage differentiation, but not obesity, modulates intrinsic *GDF15* expression

To examine whether obesity regulates *Gdf15* expression in macrophages, we sorted ATMs from mice fed either a chow or HFD for 12 weeks. No difference in *Gdf15* expression was observed in either ATMs or any other fractions of epiAT between chow and HFD-fed mice (Fig. 3F). Since the whole epiAT has been fractionated and none of the purified fractions showed any changes in *Gdf15* expression, an alteration of the ratio between fractions likely accounts for the increase of *Gdf15* expression observed in the whole tissue. As already reported[30], a major enrichment in macrophage content occurred in SVF with HFD (Supplementary Fig. 3I, K), suggesting that the increase of *Gdf15* expression in epiAT during obesity is not related to an increase of its expression in ATMs, but likely results from the accumulation of macrophages which express high *Gdf15* levels.

Monocytes expressed low levels of *Gdf15* (Fig. 3C and Supplementary Fig. 3G). Since macrophage infiltration in AT partially arises from the recruitment and differentiation of circulating monocytes[1,2], we hypothesized that *Gdf15* expression may be induced during the monocyte to macrophage differentiation. To recapitulate this process, we sorted blood monocytes from naive mice and differentiated them into monocyte-derived macrophages (MDM) in vitro (Supplementary Fig. 3L–M). Monocyte differentiation into macrophages resulted in increased *Gdf15* expression and secretion (Fig. 3G–I), demonstrating that monocytes have the potential to express high amounts of GDF-15 and that *Gdf15* expression is a characteristic of mature macrophages in mice. Similar results were obtained when differentiating bone marrow cells into bone marrow-derived macrophages (BMDMs) (Supplementary Fig. 3N). The in vitro polarization of BMDMs into M1 macrophages did not modify *Gdf15* expression, while M2 polarization slightly decreased it (Supplementary Fig. 3O–P).

In VAT of patients with obesity, *GDF15* expression was higher in the SVF than in the adipocyte fraction and GDF-15 immunohistochemical staining was detected within inflammatory infiltrates and crown-like structures as in mice (Fig. 4A, B). Sorting of SVF and immunohistofluorescence confirmed predominant expression of *GDF15* by human ATMs (Fig. 4C, D and Supplementary Fig. 4A–C). The expression of macrophage markers strongly correlated with *GDF15* expression in VAT and, unlike in mice, also in SAT (Fig. 4E). Moreover, as it was the case for *GDF15* expression (Fig. 1G–H), the expression of the macrophage marker CD64 (*FCGR1A*) was higher in AT from patients with obesity and T2D compared to subjects without T2D (Supplementary Fig. 4D–E), suggesting that increased macrophage content in AT may account for increased *GDF15* expression by obesity and T2D. In line with the mouse data showing that the differentiation of monocytes into macrophages, but not obesity, promotes *Gdf15* expression; *GDF15* expression increased upon differentiation of human blood monocytes into MDMs (Supplementary Fig. 4F–G), and *GDF15* expression in ATMs from VAT did not correlate with obesity parameters (Supplementary Fig. 4H). However, as expected, ATM content in SVF correlated with obesity parameters (Supplementary Fig. 4H). M2 polarization of human MDMs reduced *GDF15* expression in vitro (Supplementary Fig. 4I–J), as also observed in mouse macrophages. Together, these results show that the expression of *GDF15* in mature macrophages is constitutively high and is not upregulated by obesity in both mice and humans. Therefore, the increased *GDF15* expression in AT during obesity and T2D likely results from a local accumulation of macrophages.

Macrophage infiltration in AT contributes to GDF-15 production in obesity

To determine whether macrophage infiltration contributes to GDF-15 production, we depleted macrophages in HFD-fed mice. Mice were sacrificed 4 days after a single injection with anti-CD115 antibody in

https://doi.org/10.1038/s41467-024-51078-2

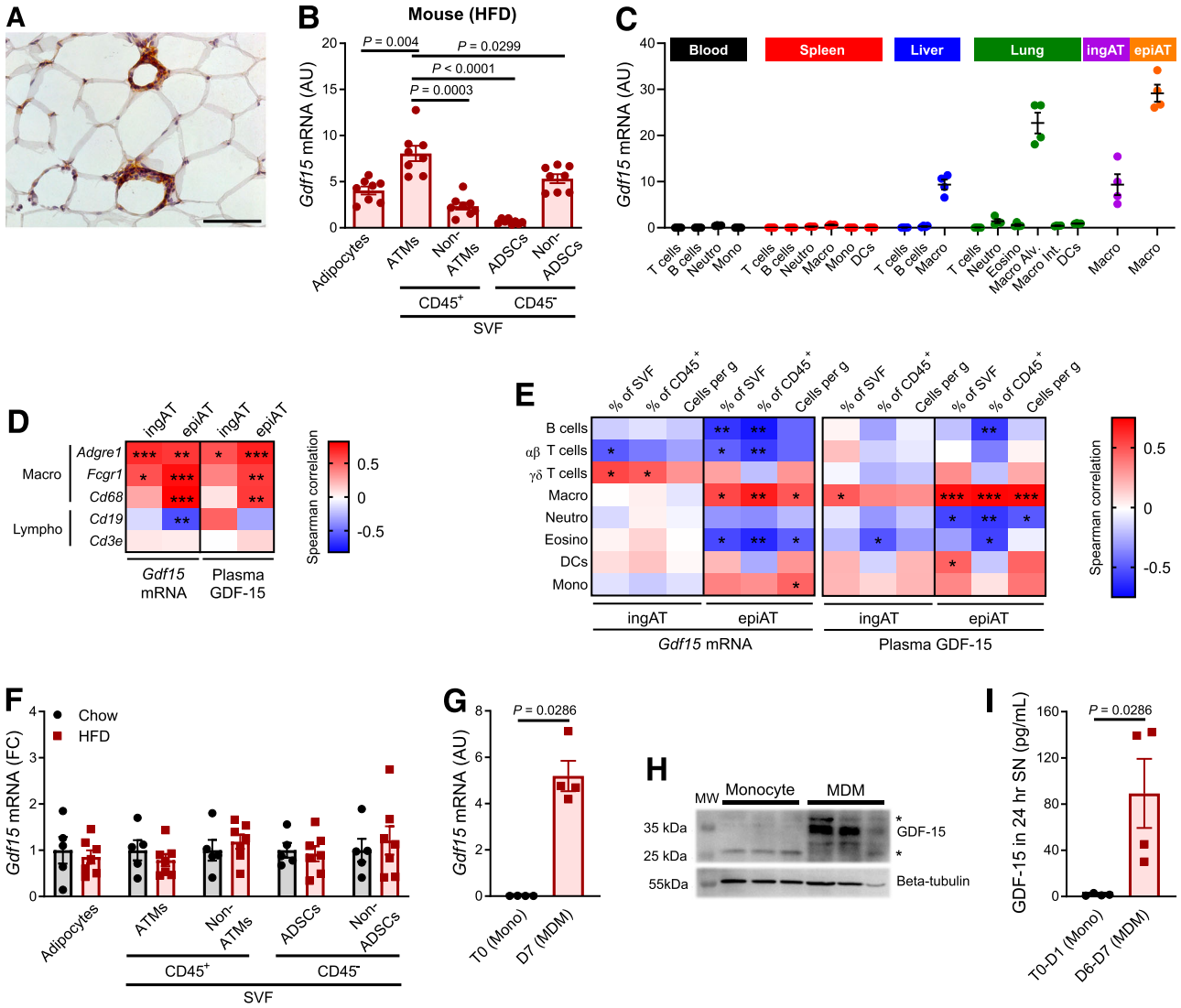

Fig. 3 | Macrophages express high levels of *GDF15* in mouse epiAT. **A** Representative immunohistochemistry of epiAT sections from HFD-fed mice stained with anti-GDF-15 antibody. Scale bars, 100 μm. **B** *Gdf15* mRNA expression levels in adipocytes and sorted SVF from epiAT of mice on HFD feeding for 12 weeks ($n = 8$). **C** *Gdf15* mRNA expression levels in the main immune cell populations sorted from several tissues of naive mice ($n = 4$). **D** Correlation between mRNA expression levels of macrophage or lymphocyte markers in AT and *Gdf15* mRNA expression levels or plasma GDF-15 concentrations in mice on chow or HFD feeding ($n = 20$). **E** Correlation between immune cell composition in AT determined by flow cytometry and *GDF15* mRNA expression levels in the corresponding tissue or plasma GDF-15 concentrations in mice on chow or HFD feeding ($n = 19$). **F** Mice were fed a chow ($n = 5$) or a HFD ($n = 7$) for 12 weeks and epiAT were processed for cell sorting. *Gdf15* mRNA expression levels were measured in adipocytes and sorted SVF. **G**–**I** Mouse blood monocytes were differentiated in monocyte-derived macrophages (MDM) by stimulation with M-CSF for 7 days ($n = 3$-4). **G** *Gdf15* mRNA expression levels in freshly sorted monocytes (T0) or in fully differentiated MDM (D7) ($n = 4$). **H** GDF-15 protein levels detected by western blot in freshly sorted monocytes or in fully differentiated MDM ($n = 3$). Nonspecific bands are indicated with a *. Uncropped blot in Source Data. **I** Secretion of GDF-15 in supernatant (SN) during the first (T0-D1) and the last (D6-D7) 24 h ($n = 4$). Data are shown as mean ± SEM. *P* values calculated by Friedman test followed by two-stage linear step-up procedure of Benjamini, Krieger and Yekutieli (**B**), two-tailed Spearman correlation (**D**, **E**), 2-way ANOVA followed by Sidak's multiple comparisons test (**F**) or two-tailed Mann–Whitney test (**G**, **I**). *$P < 0.05$; **$P < 0.01$; ***$P < 0.001$; AU arbitrary unit, SVF stromal vascular fraction, ADSCs adipose-derived stem cells, FC fold change. Source data are provided as a Source Data file.

order to achieve an acute depletion without overt effects on body weight (Supplementary Fig. 5A–C). Treatment with the anti-CD115 antibody successfully decreased macrophage content in both epiAT and ingAT without altering other immune cells (Fig. 5A and Supplementary Fig. 5D–E). Macrophage depletion reverted obesity-induced *Gdf15* expression in epiAT, but did not affect *Gdf15* expression in chow-fed mice (Fig. 5B), demonstrating that macrophage infiltration regulates the obesity-dependent elevation of *Gdf15* expression in epiAT.

Further, we prepared glucan-encapsulated RNAi particles (GeRPs) to specifically deliver *Gdf15* siRNA into ATMs. The silencing efficiency of *Gdf15* siRNA and si*Gdf15*-GeRPs was first validated in vitro (Supplementary Fig. 6A, B). As previously reported[32], intraperitoneally injected GeRPs have a strong tropism for epiAT and GeRPs were only taken up by phagocytic cells such as macrophages, neutrophils, DCs and monocytes (Supplementary Fig. 6C, D). A significant decrease in *Gdf15* expression was only observed in ATMs (Fig. 5C). We hypothesize this is due to both low *Gdf15* expression in non-macrophage phagocytes and limited GeRPs uptake in other cell populations in epiAT. Similar to macrophage depletion, macrophage-specific silencing of *Gdf15* reduced obesity-induced *Gdf15* expression in epiAT (Fig. 5D). Moreover, mice injected with si*Gdf15*-GeRPs also showed a decrease in plasma GDF-15 concentrations (Fig. 5E), demonstrating that ATMs

https://doi.org/10.1038/s41467-024-51078-2

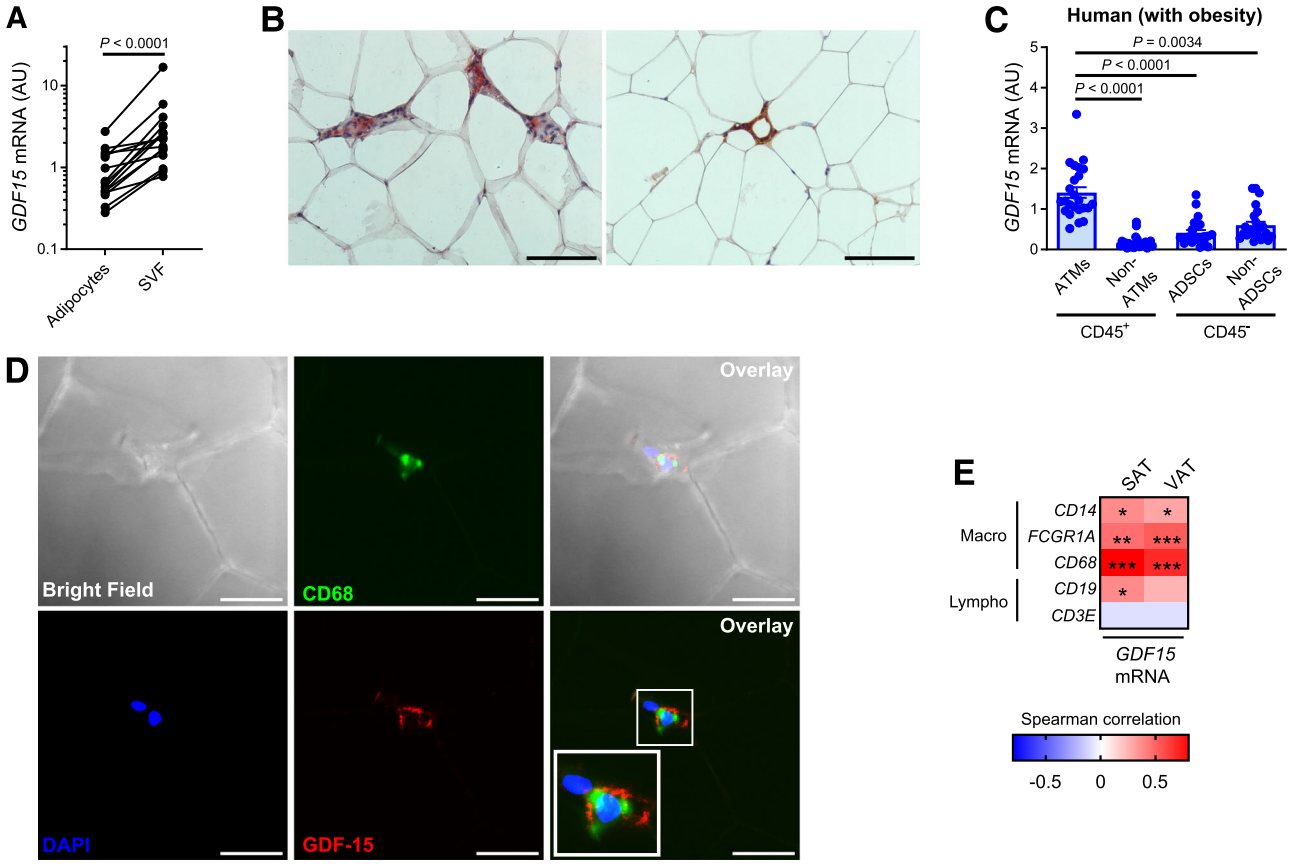

Fig. 4 | ATMs are the main source of GDF-15 in human AT. A *GDF15* mRNA expression levels in adipocytes and SVF isolated from VAT of patients with obesity ($n = 15$). Connected dots represent fractions from the same patient. **B** Representative immunohistochemistry of VAT sections from patients with obesity stained with anti-GDF-15 antibody. Scale bars, 100 μm. **C** *GDF15* mRNA expression levels in sorted SVF from VAT of patients with obesity ($n = 24$). **D** Representative immunofluorescence staining of VAT section from a patient with obesity stained with anti-GDF-15 and anti-CD68 antibodies. Scale bars, 30 μm. **E** Correlation between *GDF15* mRNA expression levels and mRNA expression levels of macrophage or lymphocyte markers in paired SAT and VAT from patients ($n = 42$). Data are shown as mean ± SEM. *P* values calculated by two-tailed Wilcoxon matched-pairs signed rank test (**A**), Kruskal–Wallis test followed by Dunn's multiple comparisons test (**C**) or two-tailed Spearman correlation (**E**). $^{*}P < 0.05$; $^{**}P < 0.01$; $^{***}P < 0.001$; AU arbitrary unit, SVF stromal vascular fraction, ADSCs adipose-derived stem cells. Source data are provided as a Source Data file.

contribute to circulating GDF-15 levels during obesity. Repeated injections of β-glucan-based particles induced body weight loss (Supplementary Fig. 6E), but mice injected with si*Gdf15*-GeRPs maintained a higher body weight than mice injected with siCtrl-GeRPs (Fig. 5F), suggesting that macrophage production of GDF-15 has a functional impact on body weight, in agreement with the anorectic action of GDF-15[8,9,13,14,18,20,33].

To confirm the functional contribution of ATMs to GDF-15 production in obesity, we transplanted bone marrow from *Gdf15*$^{+/+}$ and *Gdf15*$^{-/-}$ mice into *Gdf15*$^{+/+}$ recipient mice (Supplementary Fig. 7A). No differences between genotypes were observed in body weight after bone marrow transplantation (BMT) (Supplementary Fig. 7B). After 12 weeks of HFD feeding, *Gdf15*$^{-/-}$ BMT mice gained more weight and fat mass was higher than *Gdf15*$^{+/+}$ BMT mice (Fig. 5G, H and Supplementary Fig. 7C). Fasting glucose and insulin concentrations were not significantly affected, but *Gdf15*$^{-/-}$ BMT mice displayed higher liver steatosis compared to *Gdf15*$^{+/+}$ BMT mice (Supplementary Fig. 7D–I), likely related to the higher level of obesity. Cumulative food intake was higher in *Gdf15*$^{-/-}$ BMT mice than *Gdf15*$^{+/+}$ BMT mice upon HFD feeding (Supplementary Fig. 7J–K). Similar to the results obtained following macrophage depletion and si*Gdf15*-GeRPs experiments, *Gdf15*$^{-/-}$ BMT mice did not show obesity-induced elevation of *Gdf15* expression in epiAT (Fig. 5I). Surprisingly, no differences in plasma GDF-15 concentrations were observed at the time of sacrifice at 12 weeks (Fig. 5J). However, *Gdf15*$^{-/-}$ BMT mice exhibited lower plasma GDF-15 concentrations at 4 weeks of HFD feeding compared to *Gdf15*$^{+/+}$ BMT mice which fades at 8 weeks, suggesting that ATM-driven AT production of GDF-15 mostly occurs in early stages of obesity. Importantly, differences in plasma GDF-15 concentrations at 4 weeks coincided with the period of accelerated weight gain in *Gdf15*$^{-/-}$ BMT mice. Since HFD feeding also increased *Gdf15* expression in liver (Fig. 1B), we measured hepatic *Gdf15* expression. While hepatic *Gdf15* expression was higher upon HFD feeding, no difference in expression was observed in liver between *Gdf15*$^{-/-}$ BMT mice and *Gdf15*$^{+/+}$ BMT mice (Fig. 5K). Together these results show that ATMs contribute to plasma GDF-15 levels early during obesity development in mice and that ATM-produced GDF-15 reduces body weight gain. However, at later stages of obesity, the liver likely contributes to circulating GDF-15 concentrations as well, similarly to what we observed in humans during MASLD progression.

Hepatocytes increase *GDF15* expression during MASLD development

The foregoing BMT experiment suggests that macrophages are not involved in GDF-15 production by the liver. Indeed, macrophage depletion with the anti-CD115 antibody did not prevent the increase of hepatic *Gdf15* expression observed in mice fed either HFD or CDAA diet (Fig. 6A, B and Supplementary Fig. 8A, B). Moreover, *GDF15* expression was not associated with expression of macrophage markers in human liver (Fig. 6C), unlike in AT (Fig. 4E).

https://doi.org/10.1038/s41467-024-51078-2

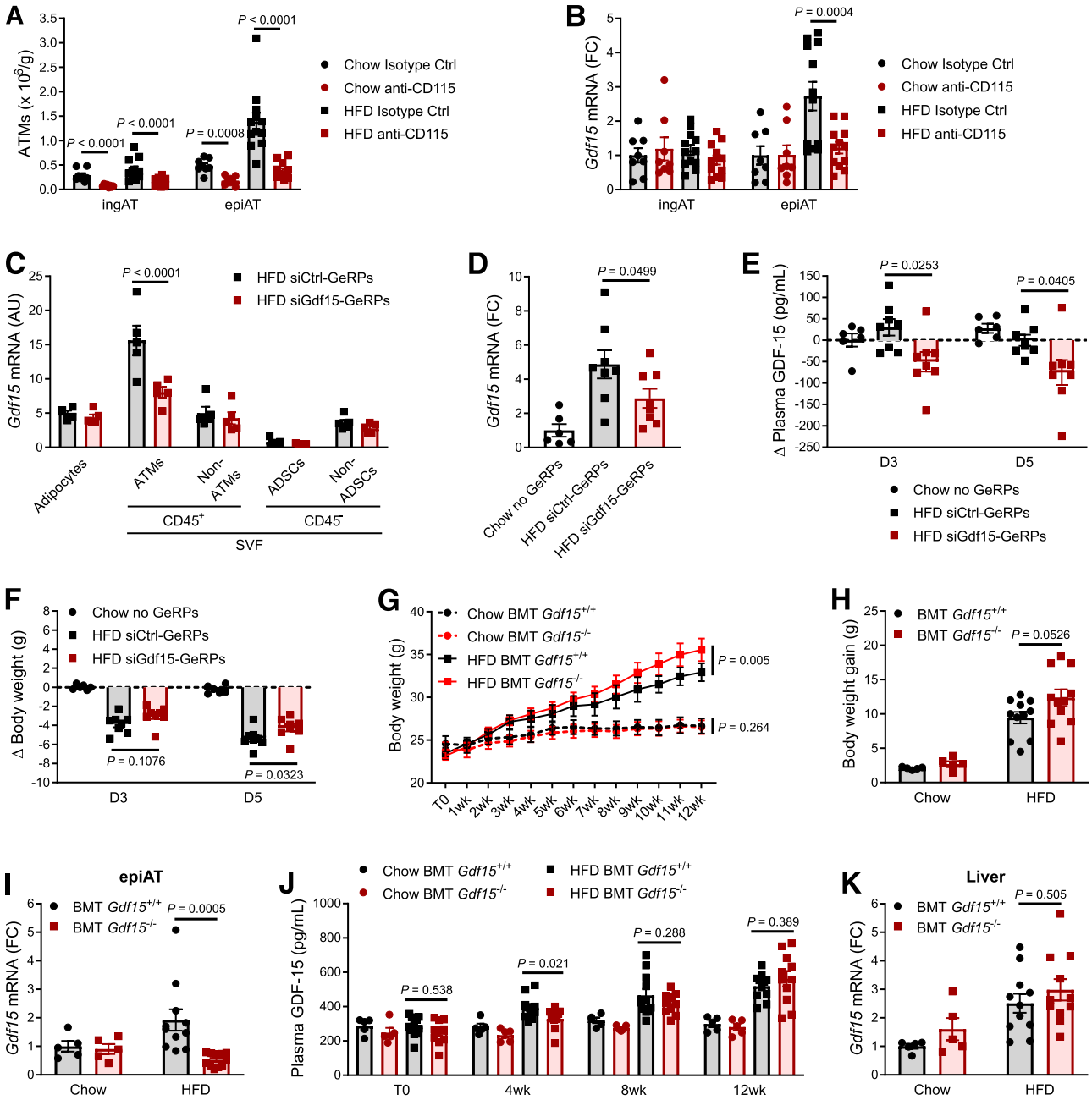

Fig. 5 | Macrophage infiltration regulates GDF-15 production by AT. A, B Mice were fed a chow or a HFD for 12 weeks followed by a single intraperitoneal injection of anti-CD115 antibody or isotype control ($n = 8$ chow and 12 HFD/antibody). Mice were sacrificed after 4 days. **A** ATM content determined by flow cytometry. **B** *Gdf15* mRNA expression levels in AT. **C–F** Mice were fed a chow ($n = 6$) or a HFD ($n = 16$) for 18 weeks followed by intraperitoneal injection of si*Gdf15*-GeRPs or siCtrl-GeRPs for 5 consecutive days ($n = 8$/siRNA-GeRPs). Mice were sacrificed 24 h after the last injection. **C** *Gdf15* mRNA expression levels in adipocytes or sorted SVF from epiAT ($n = 5$/group). **D** *Gdf15* mRNA expression levels in epiAT. **E** Difference in plasma GDF-15 concentrations after 3 days or at sacrifice (D5) compared to T0. **F** Difference in body weight after 3 days or at sacrifice (D5) compared to T0. **G–K** After bone marrow transplantation (BMT) from *Gdf15*$^{+/+}$ or *Gdf15*$^{-/-}$ mice, reconstituted mice were fed a chow or a HFD for 12 weeks ($n = 5$ chow and 11 HFD/genotype). **G** Evolution of body weight. Statistical analysis is only shown for the factor "genotype" (*Gdf15*$^{+/+}$ or *Gdf15*$^{-/-}$) calculated by 2-way ANOVA. **H** Body weight gain (12th week minus T0). **I** *Gdf15* mRNA expression levels in epiAT. **J** Plasma GDF-15 concentrations. **K** *Gdf15* mRNA expression levels in liver. Data are shown as mean ± SEM. *P* values calculated by 2-way ANOVA followed by Holm-Sidak's (**A**, **G**, **J**) or Sidak's (**B**, **C**, **E**, **F**, **H**, **I**, **K**) multiple comparisons test or two-tailed Mann–Whitney test (**D**). AU, arbitrary unit; FC, fold change. Source data are provided as a Source Data file.

To identify the cellular source of GDF-15 in liver, hepatocyte and non-parenchymal cell (NPC) fractions were isolated from naive mouse liver. *Gdf15* expression was higher in hepatocytes than NPCs (Fig. 6D and Supplementary Fig. 8C, D). Immunohistological staining of GDF-15 on human liver sections was also widely positive in hepatocytes (Supplementary Fig. 8E). As observed in whole liver, *Gdf15* expression predominantly increased in the hepatocyte fraction from mice fed steatohepatitis-inducing diets, i.e., HFSCD and CDAA (Fig. 6E), suggesting that the elevation of *GDF15* expression in liver during MASLD development results mostly from an increase of its expression in hepatocytes. However, the additional contribution of other liver cell types than hepatocytes cannot be totally excluded.

Hepatocyte-specific siRNA-driven inactivation[34] of *Gdf15* decreased *Gdf15* expression in whole liver of CDAA-fed mice (Fig. 6F), but not in

https://doi.org/10.1038/s41467-024-51078-2

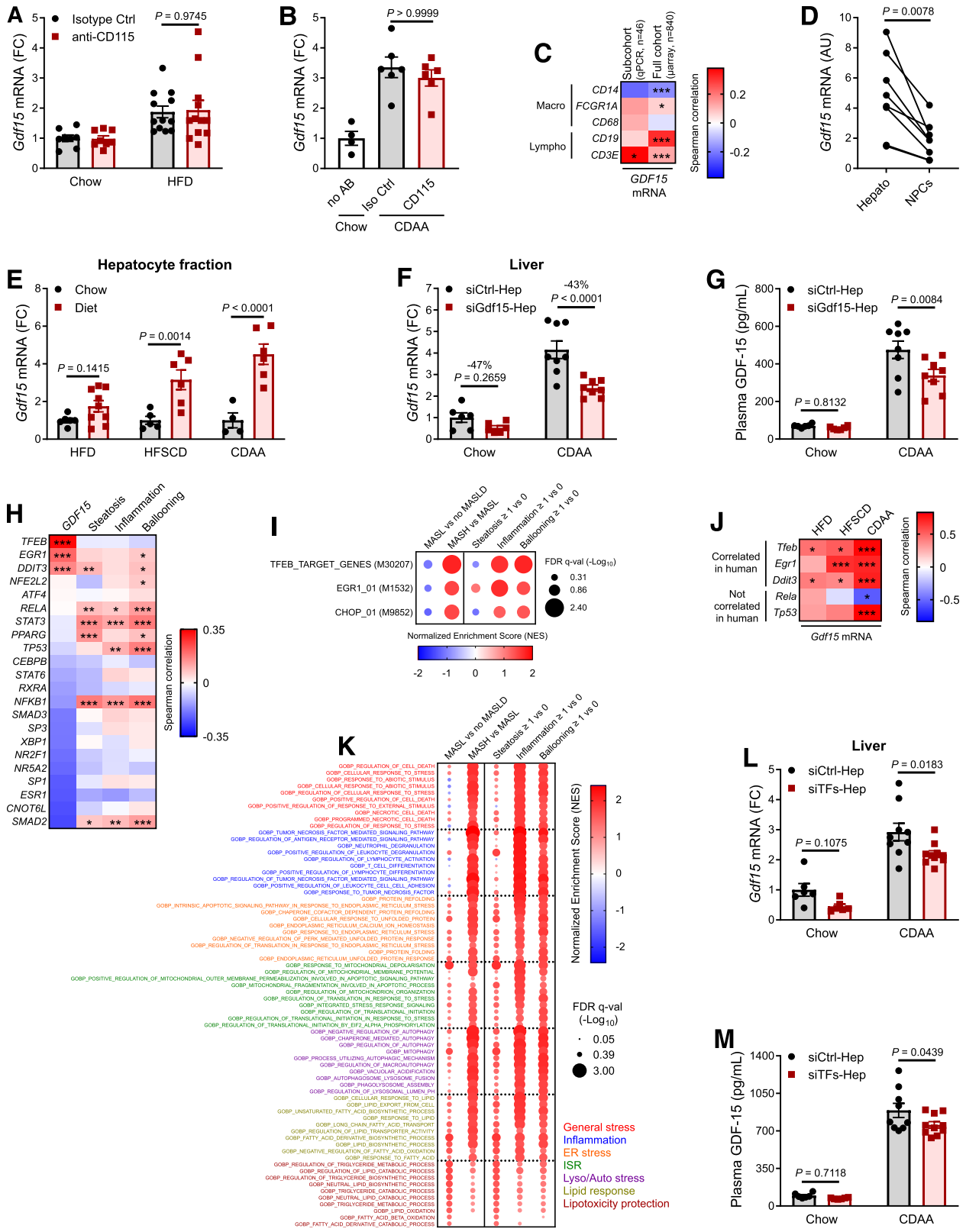

other tissues expressing high levels of *Gdf15*, including AT and kidney (Supplementary Fig. 8F). Moreover, the reduced *Gdf15* expression in liver was associated with a decrease in plasma GDF-15 concentrations (Fig. 6G and Supplementary Fig. 8G), demonstrating the contribution of hepatocyte-derived GDF-15 to the systemic increase of GDF-15 in MASH. Interestingly, CDAA-fed mice with hepatocyte *Gdf15* inactivation gained slightly more weight than control mice (Supplementary Fig. 8H, I), suggesting a role of increased hepatic *Gdf15* expression in CDAA-induced weight loss.

MASLD-associated stress induces GDF-15 in hepatocytes

To identify potential regulators of *GDF15* expression in hepatocytes, we searched for an association between hepatic *GDF15* expression and the expression of genes encoding proteins involved in the regulation

Fig. 6 | MASH-related stress increases *GDF15* expression in hepatocytes. Mice were fed a HFD for 12 weeks (**A**) ($n = 40$) or CDAA diet for 4 weeks (**B**) ($n = 16$) followed by injection of anti-CD115 antibody or isotype control. *Gdf15* mRNA expression was measured in liver. **C** Correlation between *GDF15* mRNA expression levels and mRNA expression levels of macrophage/lymphocyte markers in liver. **D** *Gdf15* mRNA expression levels in hepatocytes and non-parenchymal cells (NPCs) from naive mice ($n = 8$). Connected dots represent fractions from the same mouse. **E** *Gdf15* mRNA expression levels in hepatocytes from mice on different diet feeding ($n = 36$). **F**, **G** Mice were fed a CDAA diet for 4 weeks and tail vein injected with invivofectamine-siRNA complex prior sacrifice ($n = 28$). **F** *Gdf15* mRNA expression levels in liver. **G** Plasma GDF-15 concentrations. **H** Correlation between mRNA expression levels of GDF-15 regulators and *GDF15* mRNA expression levels, steatosis, inflammation or ballooning in liver of patients with obesity ($n = 840$). **I** GSEA of TFEB, EGR1 and DDIT3 (CHOP) signatures in liver of patients with obesity according to MASLD parameters ($n = 840$). **J** Correlation between mRNA expression levels of TFs regulating *Gdf15* with *Gdf15* mRNA expression levels in liver from mice on different diet feeding ($n = 20$/diet). **K** GSEA of stress signatures in liver of patients with obesity according to MASLD parameters ($n = 840$). Ten pathways for each type of stress are illustrated. Full analysis in Supplementary Fig. 9. **L**, **M** Mice were fed a CDAA diet for 4 weeks and tail vein injected with invivofectamine-siRNA complex prior sacrifice ($n = 31$). **L** *Gdf15* mRNA expression levels in liver. **M** Plasma GDF-15 concentrations. Data are shown as mean ± SEM. *P* values calculated by 2-way ANOVA followed by Holm-Sidak's multiple comparisons test (**A**, **E**–**G**, **L**, **M**), Kruskal–Wallis test followed by Dunn's multiple comparisons test (**B**), two-tailed Spearman correlation (**C**, **H**, **J**) or two-tailed Wilcoxon matched-pairs signed rank test (**D**). $^{*}P < 0.05$; $^{**}P < 0.01$; $^{***}P < 0.001$; FC, fold change; AU, arbitrary unit. Source data are provided as a Source Data file.

of *GDF15* transcription or mRNA stability. We observed that the expression of three transcription factors (TFs) (*TFEB*, *EGR1* and *DDIT3*) highly correlated with *GDF15* expression in human liver (Fig. 6H). Both *EGR1* and *DDIT3* expression were higher in patients with MASH, but not *TFEB* (Supplementary Fig. 8J–L). While EGR1 and DDIT3 are mostly transcriptionally regulated, TFEB is sequestered in the cytoplasm and requires post-translational modifications to translocate into the nucleus and regulate gene expression[35]. To assess the transcriptional activity of these TFs, we performed a gene set enrichment analysis (GSEA) of their target genes in liver. We observed a strong enrichment of the three TF target gene sets in patients with MASH, but not in patients with MASL (Fig. 6I). Although TFEB expression was not increased in patients with MASH, its target genes were enriched (NES = 1.73; FDR q-val = 0.004), suggesting a higher TFEB transcriptional activity. In mice, the same three TFs were also associated with *GDF15* expression in whole liver (Fig. 6J). Unlike in humans, liver expression of these three TFs progressively increased in diet models ranging from steatosis to steatohepatitis (Supplementary Fig. 8M–O). However, only *Tfeb* and *Ddit3* were increased in the hepatocyte fraction (Supplementary Fig. 8P–R).

Importantly, the transcriptional activities of *TFEB*, *EGR1* and *DDIT3*, as assessed by GSEA of their target genes, were strongly and specifically enriched in patients with inflammation and ballooning (Fig. 6I), the two parameters defining the transition from steatosis to MASH and corresponding to the disease stage when *GDF15* expression is induced in liver. Since both inflammation and ballooning are hallmarks of cellular stress in hepatocytes and considering the fact that TFEB, EGR1 and DDIT3 are stress-responsive TFs, it is reasonable to hypothesize that the increase of *GDF15* expression may result from hepatocyte stress. Moreover, among the cellular processes that might contribute to the transition from steatosis to MASH, inflammation, ER stress, integrated stress response (ISR), lysosomal/autophagy stress and lipotoxicity are all susceptible to induce and/or activate TFEB, EGR1 and DDIT3[35–37]. Supporting this hypothesis, we observed a strong enrichment of these stress-related pathways in the liver transcriptome of patients with MASH, inflammation and ballooning, but not with MASL (Fig. 6K and Supplementary Fig. 9A, B). Furthermore, the induction of inflammation, ER stress, ISR, lysosomal/autophagy stress and lipotoxicity using TNF-α, IL-1β, lipopolysaccharide (LPS), tunicamycin, salubrinal, NH_4Cl, chloroquine (CQ) and stearate (C18:0), all increased to different extents *GDF15* expression in immortalized human hepatocytes (IHH) in vitro (Supplementary Fig. 10A), indicating that these sources of stress may potentially be involved in *GDF15* regulation in vivo. Inflammatory stimuli induced the weakest *GDF15* expression, while ER stress or its downstream ISR both triggered a robust increase of *GDF15* expression (Supplementary Fig. 10A). C18:0, a saturated fatty acid displaying lipotoxicity in vitro, increased *GDF15* expression, but not the monounsaturated fatty acid oleate (C18:1) which does not induce toxicity at equal concentrations (Supplementary Fig. 10A, B). However, both fatty acids triggered lipid droplet accumulation in hepatocytes (Supplementary Fig. 10C), showing that cellular stress, rather than steatosis, induces *GDF15* expression.

To assess the role of TFEB, EGR1 and DDIT3 in stress-induced *GDF15* expression, we silenced these TFs in vitro using specific siRNAs followed by treatment with the most potent stressors for each type of stress in IHHs (Supplementary Fig. 10D–F). TFEB silencing reduced *GDF15* expression induced by a wide range of stimuli including TNF-α, tunicamycin, salubrinal, chloroquine and stearate (Supplementary Fig. 10G). DDIT3 silencing reduced *GDF15* expression induced by tunicamycin, salubrinal and stearate, but not by TNF-α or chloroquine (Supplementary Fig. 10G), three conditions robustly increasing *DDIT3* expression in vitro (Supplementary Fig. 10F). In contrast to TFEB and DDIT3, EGR1 silencing did not demonstrate an effect on any stimuli tested (Supplementary Fig. 10G). As previously reported[38], DDIT3 regulates *EGR1* expression (Supplementary Fig. 10E), which may explain the similar pattern of correlations between EGR1 and DDIT3 (Fig. 6H), as *EGR1* expression may reflect *DDIT3* expression and transcriptional activity. Supporting this hypothesis, we indeed observed an association between *DDIT3* and *EGR1* expression in the liver transcriptome (Spearman r 0.1349; *P* value < 0.0001). In vivo, combined inactivation of *Tfeb* and *Ddit3* in hepatocytes decreased hepatic *Gdf15* expression and plasma GDF-15 concentrations in CDAA-fed mice (Fig. 6L, M and Supplementary Fig. 11A–D). Silencing of the two TFs in CDAA-fed mice tended to increase weight gain compared to the control mice, but this did not reach statistical significance (Supplementary Fig. 11E, F). Altogether, our results show that *GDF15* expression is increased in hepatocytes during the transition from steatosis to MASH. GDF-15 production likely results from the development of several stresses in hepatocytes that activate TFEB and DDIT3, two stress-responsive TFs regulating *GDF15* transcription.

Discussion

Using different mouse models of obesity and MASLD as well as biopsies from carefully-characterized patients, we identify a progressive increase in GDF-15 starting in AT at the onset of obesity and T2D, followed by liver during the progression toward MASH. Obesity, in the absence of T2D and MASLD, is intrinsically associated with an increase of *GDF15* expression in AT and plasma GDF-15 concentrations. Although an earlier study reported no difference in *GDF15* expression in both SAT and VAT on a small cohort of patients with obesity[21], we observed a clear increase in *GDF15* expression in AT in two independent human cohorts and in two mouse models of obesity. The increase in *GDF15* expression mostly occurs in VAT and to a lesser extent in SAT from patients with obesity. Moreover, progression to T2D further increases *GDF15* expression in AT and plasma GDF-15 concentrations. GFRAL, the sole known GDF-15 receptor, is mostly expressed in brainstem structures and scarcely expressed in peripheral tissues. As extensively reported, GDF-15 protects against obesity through the binding and activation of its receptor GFRAL in the central nervous system[8,9,33]. Obesity has no impact on *GFRAL* expression in peripheral

tissues, suggesting that the elevation of GDF-15 is the major peripheral alteration in the GDF15-GFRAL pathway.

The exploration of human VAT and mouse epiAT revealed that macrophages express the highest level of *GDF15* in these tissues. Extensive analysis of the immune cell populations showed that *Gdf15* expression is essentially limited to macrophages. A large heterogeneity of *Gdf15* expression was observed in macrophages according to tissue origin with macrophages from epiAT expressing more than those from ingAT or liver. Circulating monocytes display low *Gdf15* expression, but its expression strongly increases during their differentiation into macrophages, showing that GDF-15 production is a characteristic of mature macrophages in certain tissular contexts. M2 polarization or the tissue resident phenotype, which share several phenotypical characteristics, are associated with a lower *Gdf15* expression. However, no difference in *Gdf15* expression was observed in the whole macrophage population with obesity, suggesting that macrophage recruitment/differentiation predominates over polarization or the macrophage subtype. Indeed, macrophage infiltration in AT is strongly associated with *GDF15* expression in both humans and mice. Macrophage depletion or *Gdf15* silencing in macrophages prevents obesity-induced *Gdf15* expression in epiAT. Acute silencing of *Gdf15* in macrophages by si*Gdf15*-GeRPs reduces plasma GDF-15 concentrations in obese mice. The chronic silencing of *Gdf15* in macrophages obtained in *Gdf15*$^{-/-}$ BMT mice decreases plasma GDF-15 concentrations in early-onset of obesity and exacerbates obesity. At later stages, the difference in circulating GDF-15 concentrations disappears, likely because *Gdf15*$^{-/-}$ BMT mice develop a more severe obesity, including more advanced liver complications. Indeed, the development of MASLD leads to the production of GDF-15 by the liver which might progressively attenuates the difference in plasma GDF-15 levels observed at early stages in *Gdf15*$^{-/-}$ BMT mice. These results show that ATMs not only contribute to the systemic rise of GDF-15 in early stages of obesity, but also that ATMs play an unexpected role in body weight regulation. ATMs are widely considered as detrimental in obesity, mostly because of their production of pro-inflammatory factors contributing to metabolic complications of obesity such as T2D[1,2]. However, ATMs also play protective functions during obesity such as helping adipocytes to handle excessive lipids and clearing dead adipocytes[1]. The production of GDF-15 and its anti-obesity effect that we describe here, further illustrates the beneficial role of ATMs in obesity. As a consequence, targeting macrophage inflammatory pathways rather than preventing macrophage infiltration is likely to be more effective in treating obesity and its complications.

It was previously suggested that the liver is the primary source of GDF-15 in mouse models of obesity[17,19,26]. However, feeding mice with HFD for 12 to 24 weeks, as performed in these studies, leads to severe obesity, insulin resistance and MASLD-like conditions, making difficult to properly identify the specific contribution of each of these conditions. Here we observe that 12 weeks of HFD feeding does indeed increases the expression of *Gdf15* in liver, in addition to epiAT. However, human livers only show increased *GDF15* expression in correlation with MASLD severity, and not with obesity or T2D. In patients with obesity but without MASLD, plasma GDF-15 concentrations increase while *GDF15* expression in liver does not, excluding a role of liver in obesity-related GDF-15 elevation. Subsequent to MASLD development, *GDF15* expression progressively increases in liver and reaches the highest level in patients with MASH. The emergence of MASH in patients with obesity is associated with a major elevation of GDF-15 levels, demonstrating that MASH is a substantial additional factor contributing to GDF-15 elevation and that liver production might exceed the production from adipose tissue in advanced stages of MASLD. Similarly, the induction of obesity-independent MASH-like condition in mice with CDAA diet also leads to a robust increase of plasma GDF-15 concentrations. Altogether, these results show that *GDF15* expression in liver is not directly affected by obesity, but follows the development of MASLD and particularly its severe form MASH.

Although MASH is an inflammatory condition characterized by immune cell infiltration in the liver[39], macrophages are not the source of MASH-induced *Gdf15* expression in liver. Hepatocytes, the main parenchymal cell type in liver, mostly express *GDF15* and upregulate their expression according to the development of MASH-like conditions in mice. *GDF15* expression in our liver transcriptomic cohort is strongly associated with the expression of *TFEB* and *DDIT3*, two genes encoding for stress-responsive TFs. A systemic and in-depth analysis of all the gene sets derived from the GO Biological Process revealed an enrichment in patients with MASH of several stresses able to activate TFEB and DDIT3, including inflammation, ER stress, ISR, lysosomal/autophagy stress and lipotoxicity. The induction of these stresses in vitro upregulates *GDF15* expression in hepatocytes, with ER stress, ISR and lipotoxicity exerting the most potent effects, while inflammation and lysosomal/autophagy stresses display a limited impact on *GDF15* expression. Knockdown of TFEB reduces *GDF15* expression by all of these stresses, while knockdown of DDIT3 specifically reduces *GDF15* expression by ER stress, ISR and lipotoxicity. In vivo, the combined hepatic inactivation of *Tfeb* and *Ddit3* decreases *Gdf15* expression and plasma GDF-15 concentrations in CDAA-fed mice. The modest induction of *GDF15* expression by inflammatory stimuli in vitro and the limited increase of *GDF15* expression in livers of patients with obesity, steatosis and inflammation, but without ballooning, suggest that inflammation per se likely plays a minor role on the elevation of *GDF15* expression in liver. The excessive accumulation of lipids in hepatocytes during MASLD development disrupts lipid homeostasis and favors the generation of toxic lipid species[3]. The resulting lipotoxicity promotes organelle dysfunction and contributes to the development of lysosomal/autophagy stress, ER stress and ISR[4]. These stresses are tightly inter-connected in MASH and likely contribute together to induce *GDF15* expression in liver. Interestingly, other types of experimental liver injuries such as those induced by CCl_4, ethanol, D-galactosamine, partial hepatectomy or acetaminophen also increase *Gdf15* expression in mouse liver[40,41]. While most of these models are not associated to lipotoxicity, they induce different levels of lysosomal/autophagy stress, ER stress and ISR[42–48], suggesting that the upregulation of *GDF15* expression in liver is not specific to MASH but seems broadly related to hepatocyte stress.

Previous studies have identified circulating GDF-15 level as a predictive factor for developing T2D[22,49] and MASH[23]. Since macrophage accumulation in AT contributes to the development of insulin resistance[2] and macrophages are the main source of GDF-15 in AT, circulating GDF-15 levels can indirectly inform about the extent of macrophage infiltration in AT and therefore about the risk of developing T2D. Similarly, as GDF-15 is mostly produced by liver in MASH, increased plasma GDF-15 levels can also be indicative of MASH development. Circulating GDF-15 levels may therefore be seen as a broad biomarker for metabolic risk.

As GDF-15 protects against weight gain, the increase in plasma concentration during obesity might seem paradoxical. However, elevated plasma GDF-15 is not restricted to obesity, but is also observed in a wide range of chronic diseases including cancer[50] and cardiovascular diseases[51]. Mechanistically, we demonstrate that macrophage infiltration and various cellular stresses promote GDF-15 production in the course of obesity and its complications. Interestingly, macrophage infiltration and cellular stress are two common processes occurring in most chronic diseases. It would be of interest to examine whether these two distinct mechanisms may also be at play in other pathophysiological conditions.

GDF-15 is an attractive target for treating obesity and several GDF-15 analogs demonstrated promising results in pre-clinical models of obesity[8–10,33,52,53]. However, they are all based on recombinant GDF-15 and require regular injections due to the short half-life of GDF-15.

Rather than directly providing GDF-15 analogs, increasing endogenous production of GDF-15 by small molecules may represent a promising alternative. In this context, TFEB and DDIT3 may represent new potential targets. Interestingly, the delivery of small-molecule TFEB agonists in obese mice reduces body weight gain[54].

Altogether, these results highlight the complexity of GDF-15 regulation in metabolic diseases and reveal the distinct involvement of immune and non-immune actors in this process. In obesity, the accumulation of macrophages in AT triggers GDF-15 elevation, a process exacerbated when coexisting with T2D. MASH is an additional and independent factor further increasing GDF-15 production via hepatocytes experiencing cellular stress. These findings prompt us to rather consider GDF-15 as a stress-responsive cytokine linked with both inflammation and cellular stress, two processes highly common in many pathophysiological conditions that may account for the elevation of GDF-15 in a broad range of other diseases.

Methods

The present research complies with all relevant ethical regulations. All human procedures were ethically approved by the Comité de Protection des Personnes Nord Ouest IV or by the ethics committee of Liège University Hospital. The analysis performed in this study aligned with the original scopes and objectives of the ABOS and Liège cohort studies and no additional ethic approval was therefore requested. All animal procedures were approved by the ethical committee for animal experimentation of the Nord-Pas-de-Calais Region (CEEA75).

Human studies

Patients enrolled in the present study were participants of the Biological Atlas of Severe Obesity (Atlas Biologique de l'Obesité Sévère [ABOS]) cohort (ClinicialTrials.gov: NCT01129297) and were recruited at the Centre Hospitalier Universitaire de Lille (France), as previously described[55,56]. Briefly, subcutaneous adipose tissue (SAT, abdominal wall), visceral adipose tissue (VAT, greater omentum) and liver biopsies were collected during abdominal surgery including parietal surgery, cholecystectomy and bariatric surgery. Sex of the participants was self-reported. All biological parameters were measured by routine clinical techniques. The Homeostasis Model Assessment of insulin resistance (HOMA2-IR) was calculated using the HOMA2 calculator version 2.2.3 (www.dtu.ox.ac.uk/homacalculator/). Liver histology was blindly evaluated by two pathologists by using the "NAFLD" activity score (NAS) system as recommended by the NASH Clinical Research Network[57]. Preparation of liver biopsies for microarray was previously described[58] and data are available at GEO under the accession number GSE130991. Anthropometric, biological and histological characteristics of patients are available in Supplementary Tables 1, 2 and 5.

Obesity was defined by a body mass index (BMI) ≥ 30 kg/m². T2D was defined according to the American Diabetes Association recommendation: fasting plasma glucose ≥7.0 mmol/L, glycated hemoglobin A1c (HbA1c) ≥ 6.5%, or two-hour plasma glucose ≥11.1 mmol/L during an oral glucose tolerance test[59]. Patients with at least one cardiometabolic risk factors were classified as MASLD when the steatosis score ≥1 (steatosis grade ≥5%) or MASH if the three scores ≥1 (steatosis, inflammation and ballooning), according to steatotic liver disease nomenclature[60]. All procedures were ethically approved by the Comité de Protection des Personnes Nord Ouest IV and were compliant to the French National Ethics Committee guidelines. Written informed consent was obtained from all participants. The analysis performed in this study complied with the information provided to participants and aligned with the original scope and objectives of the ABOS cohort study.

Main results were confirmed in a second cohort recruited at the University Hospital of Liège (Belgium) and previously described[61]. Collected adipose tissue depots were identical to those from ABOS cohort (abdominal wall and greater omentum). All procedures were approved by the ethics Committee of Liège University Hospital. Written informed consent was obtained from all participants. The analysis performed on the confirmation cohort complied with the information provided to participants and aligned with the original scope and objectives of the Liège cohort study. Biological characteristics of the second cohort are provided in Supplementary Table 6.

Mouse studies

C57BL/6 J mice (Charles River) were maintained at 22 °C ± 2 °C on a 12-h light/dark cycle with ad libitum access to food and water in specific pathogen-free animal facilities (Pasteur Institute of Lille PLEHTA or University of Lille EOPS2). Humidity was continuously monitored and remained in the range of 40 to 60%. Eight to ten-week-old male mice were fed a high-fat diet (HFD) with 60 kcal% fat (Research Diet cat#D12492); a choline-deficient, L-amino acid-defined (CDAA) diet with 41 kcal% fat, 35 gm% sucrose and 2 gm% cholesterol (Ssniff cat#S8840-E600 custom diet); a high-fat high-sucrose high-cholesterol diet (HFSCD) with 45 kcal% fat, 35 gm% sucrose and 1 gm % cholesterol (SAFE cat#U8954 custom diet) or maintained under chow diet (SAFE cat#A04) for the indicated time. In addition to CDAA diet, mice also received monosaccharides in the drinking water (42 g/L, fructose:glucose ratio of 55:45).

Body weight was measured weekly. Before sacrifice, mice were fasted for 4 to 5 hrs. Fasting glucose was measured with an Accu-Chek Performa Blood Glucose Meter (Roche) through tail-vein puncture. Blood was collected in EDTA-coated microvette by snipping the tail. All mice were euthanized at ZT2-3 (9-10 am) or ZT6-7 (1-2 pm) by cervical dislocation. Lipids were extracted from the liver caudate lobe by the Folch method as previously described[28] and triglycerides were measured with the triglycerides FS kit (DiaSys, #157109910026). All animal procedures were performed in accordance with European guidelines on the protection of animals used for scientific purposes (2010/63/UE) and approved by the ethical committee for animal experimentation of the Nord-Pas-de-Calais Region (CEEA75) under the following numbers: APAFIS#7738-2015121713177853, APAFIS#7160-2017040313471173, APAFIS#2017040313241087, APAFIS#11237-2017091112285145, APAFIS#32184-2021062915403703 and APAFIS #30876-2021040112094087.

Macrophage depletion

After 12 weeks of chow or 60% HFD feeding or after 4 weeks of CDAA diet feeding, mice were randomized according to their body weight and received a single intraperitoneal injection of InVivoMAb anti-mouse CSF1R (CD115) antibody (Bio X Cell cat#BE0213) or InVivoMAb rat IgG2a isotype control (clone 2A3) (Bio X Cell cat#BE0089). Each mouse received 500 μg of antibody in a volume of 150 μL. Mice were maintained on their respective diet until the sacrifice 4 days later.

GeRPs administration

GeRPs were prepared as previously described[32]. Mice were fed a 60% HFD for 18 weeks and randomized according to their body weight. FITC-labeled GeRPs were administered by intraperitoneal injections for 5 consecutive days and mice were sacrificed 24 h later. Mice received a total of 1 mg FITC-labeled glucan shells loaded with 5 nmol siRNA and 50 nM Endo-porter (Gene Tools cat#OT-EP-AQ-1). ON-TARGETplus siRNAs were order from Dharmacon (cat#D-001810-01, cat#D-001810-02, cat#J-043512-13, cat#J-043512-14, cat#J-043512-15, cat#J-043512-16) and tested in vitro in the RAW 264.7 mouse macrophage cell line transfected with Lipofectamine RNAiMAX reagent (Invitrogen cat#13778075) according to manufacturer's instructions for 32 hrs (Supplementary Fig. 6A). siRNA Ctrl_1 (cat#D-001810-01) and siRNA mGdf15_4 (cat#J-043512-16) were selected for GeRPs preparation based on the level of silencing and the reproducibility. Before in vivo experiment, the efficiency of si*Gdf15*-GeRPs was confirmed in vitro in RAW 264.7 cells (ATCC cat#TIB-71) treated with GeRPs for

32 hrs (Supplementary Fig. 6B). To validate the silencing in vivo in ATMs, five mice with the heaviest epiAT among each GeRPs group were selected for cell sorting.

Bone marrow transplantation (BMT)

Seven-week-old male C57BL/6 J mice (Charles River) were randomized according to their body weight and received a whole-body irradiation (2 × 5 Gy with 3 h apart). Five hours after complete irradiation, bone marrow cells from either *Gdf15*$^{+/+}$ (C57BL/6 J, Charles River) or *Gdf15*$^{-/-}$ (C57BL/6 J background[62]) mice were injected into the tail vein. Each irradiated mouse received 6×10^6 bone marrow cells in a volume of 200 μL. Starting 4 days before until 3 weeks after irradiation, mice were maintained on acidified water pH 2.7 with sulfatrim (0.8 mg/mL of sulfamethoxazole and 0.16 mg/mL of trimethoprim). Seven weeks after irradiation, mice were randomized according to their body weight to either a chow or a 60% HFD feeding. Mice were co-housed at a 2/2 ratio (BMT *Gdf15*$^{+/+}$/BMT *Gdf15*$^{-/-}$) for 10 weeks and single housed for the two last weeks of diet feeding to measure food intake. After 3 days of acclimation, food intake was measured by manual weighing of food using a precision scale every two days at the same time of the day (ZT7). Food spillage was low and taken into consideration.

Hepatocyte siRNA delivery

Mice were fed a CDAA diet for a total of 4 weeks. After 3 weeks of diet, body weight and plasma GDF-15 concentrations were measured to randomize mice before injections. siRNAs were delivered by using invivofectamine 3.0 reagent (Invitrogen cat#IVF3005), lipid-based nanoparticles providing high efficiency delivery of siRNA to hepatocytes following tail vein injection[34]. Invivofectamine-siRNA complexes were prepared according to the manufacturer's instructions and administered 4 days prior sacrifice. ON-TARGETplus mouse siRNA SMARTpool were ordered from Dharmacon. For *Gdf15* knock down, 1.5 mg/kg of siRNA targeting *Gdf15* (cat#L-043512-01) or non-targeting pool (cat#D-001810-10) were tail vein injected. For TFs knock down, 1.5 mg/kg of each siRNA targeting *Tfeb* (cat# L-050607-02) and *Ddit3* (cat# L-062068-00) or 3 mg/kg of non-targeting pool (cat#D-001810-10) were administered.

Cell culture and treatments

Monocyte-derived macrophages (MDMs) were generated from blood monocytes of naive mice. Blood from four to six mice was collected for each replicate and monocytes were sorted as described in cell sorting and flow cytometry section. Freshly sorted monocytes were cultured in RPMI 1640 medium (Gibco cat# 21870-092) supplemented with 20% heat-inactivated FBS (Gibco cat#10270-106), 2 mM glutamine (Gibco cat#25030-123), 40 μg/ml gentamycin (Gibco cat#15710-080) and 50 ng/mL of recombinant mouse M-CSF (Biolegend cat#576406) for 7 days at a concentration of 10^6cells/mL at 37 °C under 5% CO2 atmosphere. Medium was replaced after 3 and 6 days. A fraction of supernatant was collected after 24 h of differentiation, as well as the terminal supernatant at day 7 of differentiation, for ELISA. The proper macrophage differentiation was confirmed microscopically on an Eclipse Ti-U inverted microscope (Nikon). Human MDMs were generated from buffy coats as previously described[63]. Fully differentiated MDMs were treated with 100 ng/ml LPS (Sigma-Aldrich cat#L4391) and 20 ng/ml IFN-γ (Miltenyi Biotec cat#130-096-484) to acquire a M1-polarization or with 20 ng/ml IL-4 (ImmunoTools cat#11340043) to acquire a M2-polarization for 16 h. Mouse bone marrow-derived macrophages (BMDMs) were produced as previously described[28]. Fully-differentiated BMDMs were treated with 10 ng/ml LPS (Sigma-Aldrich cat#L4391) and 25 ng/ml IFN-γ (PeproTech cat#315-05) to acquire a M1-polarization or with 20 ng/ml IL-4 (PeproTech cat#214-14) to acquire a M2-polarization for 16 h.

Immortalized human hepatocytes[64] (IHHs) were cultured in Williams E medium (Gibco cat#22551-089) supplemented with 10% heat-inactivated FBS (Gibco cat#10270-106), 2 mM glutamine (Gibco cat#25030-123), 40 μg/ml gentamycin (Gibco cat#15710-080), 20 mU/ml bovine insulin (Sigma-Aldrich cat#I5500) and 50 nM dexamethasone (Sigma-Aldrich cat#D1756) at 37 °C under 5% CO2 atmosphere. IHHs were seeded into 24-well plates to reach 70% confluence after 48 h. Cells were treated with 1 μg/mL Tunicamycin (Sigma-Aldrich cat#T7765), 50 μM Salubrinal (Tocris cat#2347), 100 μM NH_4Cl (Sigma-Aldrich cat#A9434), 25 μM Chloroquine (Sigma-Aldrich cat#C6628), 5 ng/mL human TNF-α (Miltenyi Biotec cat#130-094-014), 10 ng/mL human IL-1β (Miltenyi Biotec cat#130-093-897), 100 ng/mL LPS (Sigma-Aldrich cat#L4391), 250 μM C18:0 (Sigma-Aldrich cat#S4751) or 250 μM C18:1 (Sigma-Aldrich cat#O1008) for 16 h. Concentrations for treatments were selected to induce minor toxicity, except for C18:0 treatment used to reproduce lipotoxicity (Supplementary Fig. 10B). Free fatty acid solutions were prepared as previously described[63]. Lipid droplet accumulation was evaluated with the lipid (Oil Red O) staining kit (BioVision cat#K580).

Cell viability assay

Cell proliferation reagent WST-1 (Roche Applied Science cat#05015944001) was used to assess cell proliferation, viability and toxicity according to the manufacturer's instructions. IHHs were seeded into 96-well plates to reach 70% confluence after 48 h. Cells were treated for 16 h before addition of WST-1 reagent. Measurement was made after 1 h of incubation on an Infinite M200 Pro system (Tecan) at 450 nm using the Magellan 7.1 SP1 software.

siRNA transfection

IHHs were seeded into 24-well plates to reach 70% confluence after 24 h. Cells were transfected by using Lipofectamine RNAiMAX reagent (Invitrogen cat#13778075) according to manufacturer's instructions. Predesigned ON-TARGETplus siRNA SMARTpool targeting human *TFEB*, *EGR1* and *DDIT3* were used (Dharmacon cat#L-009798-00-0005, cat#L-006526-00-0005 and cat#L-004819-00-0005 respectively). ON-TARGETplus Non-targeting Control Pool (Dharmacon cat#D-001810-10-05) was used as a negative control. After 32 h of transfection, medium was replaced for fresh medium containing treatments for 16 further hours before analysis.

Reverse transcription-quantitative PCR (RT-qPCR)

Total RNAs from tissues or cells were extracted with the TRIzol reagent (Ambion cat#15596018) according to manufacturer's recommendations. DNase treatment was performed by using Dnase I (Thermo Scientific cat#EN0521). Purified RNAs were reverse-transcribed to complementary DNA (cDNA) by using the high-capacity cDNA reverse transcription kit (Applied Biosystems cat#4368813). qPCR was performed by using the Low ROX SYBR MasterMix dTTP Blue (Takyon cat#UF-LSMT-B0701) and ran on a QuantStudio 3 system (Applied Biosystems) with the QuantStudio Design and Analysis v.1.5.2 software. Gene expressions were calculated using the $2^{-\Delta\Delta CT}$ method and presented as fold change (FC) or using the $2^{-\Delta CT}$ x 100 method and presented as arbitrary unit (AU). Highly stable genes were chosen as housekeeping gene; *OAZ1* and *RPLP0* for human and *Rps29* and *Rpl4* for mice[65]. Primers were designed with Primer-BLAST (NIH, https://www.ncbi.nlm.nih.gov/tools/primer-blast/) to amplify all the isoforms of the target gene. Primer sequences are provided in Supplementary Table 7.

Western blot

Cells were lysed in whole lysis buffer (62.5 mM Tris-HCl at pH 6.8, 10% glycerol, 2% SDS, 3% β-mercaptoethanol, 0.03% bromophenol blue, phosSTOP and complete protease inhibitor cocktails). After heating at 95 °C for 5 min, samples were subjected to SDS-PAGE. The following primary antibodies were used: anti-GDF15 (Novus cat#NBP2-44214) and anti-β-tubulin (Sigma-Aldrich cat#T4026). The secondary

antibodies used for the revelation were HRP-linked anti-rat IgG (Cell Signaling cat#7077) and HRP-linked anti-mouse IgG (Cell Signaling cat#7076). Revelation was performed with Pierce ECL Western Blotting Substrate (Thermo Scientific cat#32106) or SuperSignal West Femto Maximum Sensitivity Substrate (Thermo Scientific cat#34096) by using the iBright CL1500 Imaging System (Invitrogen) and its on-instrument software version 1.8.0.

ELISA

GDF-15 was quantified in plasma with the mouse GDF-15 DuoSet ELISA kit (R&D Systems, cat#DY6385-05) or the human GDF-15 DuoSet ELISA kit (R&D Systems, cat#DY957) according to the manufacturer's recommendations. Both mouse and human plasma samples were diluted 1:10. For mouse, plasma GDF-15 concentrations were measured in fasted condition when GDF-15 was only assessed in terminal but in fed condition during time course experiments, including for the last time point, always at ZT2 (9 am). For human, plasma GDF-15 concentrations were measured in fasted condition. GDF-15 concentrations were also quantified in mouse MDM supernatants with the mouse GDF-15 DuoSet ELISA kit (R&D Systems, cat#DY6385-05) without dilution.

Adipocytes and SVF separation

VAT was collected in PBS at room temperature and processed promptly. Tissue was minced with scissors and digested in RPMI containing 1 mg/mL collagenase D (Roche cat#11088882001) at 37 °C under agitation for 30 min. Cell suspension was passed five times through a 10 ml syringe with 18 G needle and then through a 100 μm cell strainer. Sample was centrifuged at 400 × *g* for 5 min at RT. Floating adipocytes were collected and lysed in TRIzol reagent. Stromal vascular fraction (SVF) pellet was incubated in ammonium chloride-based buffer (155 mM ammonium chloride, 10 mM sodium bicarbonate and 125 μM EDTA) to lyse red blood cells, washed and finally lysed in TRIzol reagent or kept for cell sorting.

Hepatocytes and NPCs separation

Livers were perfused in situ through the inferior cava vein with HBSS (Gibco cat# 14180-046) supplemented with 0.5 mM EGTA and 50 mM HEPES, followed by ~30 mL/liver of HBSS supplemented with 50 mM HEPES, 5 mM $CaCl_2$ and 0.2 mg/mL of collagenase IV (Sigma-Aldrich cat#C5138) at 37 °C. Livers were collected and dissociated with cell scrapers in Petri dishes. Cell suspension was passed through a 70 μm cell strainer and centrifuged at 50 × *g* for 2 min with reduced deceleration. Hepatocytes pellets were washed thrice with Williams E medium (Gibco cat#22551-022) and lysed in TRIzol reagent after the last centrifugation at 50 × *g*. The NPC-containing supernatants from the first centrifugation at 50 × *g* were transferred in new tubes. This step was repeated thrice to remove all remaining hepatocytes. The last NPC-containing supernatants were centrifuged at 400 × *g* for 5 min and the resulting NPC pellets were incubated in ammonium chloride-based buffer (155 mM ammonium chloride, 10 mM sodium bicarbonate and 125 μM EDTA) to lyse red blood cells, washed and finally lysed in TRIzol reagent. For livers from mice fed with HFD, HFSCD and CDAA diet, the floating fat-laden hepatocytes layer produced after the first centrifugation was also collected and pooled with the hepatocytes pellet.

Cell sorting and flow cytometry

Tissues were collected in PBS and kept on ice until processing, except for AT which has been kept at RT when adipocytes were also collected as described in adipocyte and SVF separation section. Blood was collected in EDTA blood collection tubes and kept on ice until red blood cells lysis step. Spleen was gently pressed on a 70 μm cell strainer by using the flat end of a 1 mL syringe plunger. Other tissues were minced with scissors and digested in DMEM containing 1 mg/mL collagenase D (Roche cat#11088882001) and 0.1 mg/mL of DNAse I (Roche cat#10104159001) at 37 °C under agitation for 30 min for AT, 45 min for liver and 60 min for lung. Cell suspension was passed five to ten times through a 10 ml syringe with 18 G needle (19 G needle used for liver) and then through a 70 μm cell strainer (100 μm used for AT). After centrifugation, red blood cells were lysed by incubation in ammonium chloride-based buffer. Cells were blocked by using a combination of anti-CD16/CD32 (clone 2.4G2) (BD Biosciences, cat#553142) and anti-FcγRIV (clone 9E9) (BioLegend cat#149502). Antibodies used for cell sorting and flow cytometry are provided in Supplementary Table 8.

After staining, cell suspension was directly run into an Influx cell sorter (Becton Dickinson) (Plateau d'Immunophenotypage Metabolique, Inserm U1011, Lille, France) or into a FACS ARIA III cell sorter (Becton Dickinson) (BioImaging Center Lille [BICeL], Lille, France). For human VAT, cells were sorted as illustrated in Supplementary Fig. 4A. For mouse epiAT and ingAT, cells were sorted as illustrated in Supplementary Fig. 3A. For mouse blood, the following $CD45^+$ cell populations were sorted: neutrophils ($CD11b^+$ $Ly6G^+$), T cells ($Ly6G^-$ $CD3\varepsilon^+$ $TCR\beta^+$), B cells ($Ly6G^-$ $CD3\varepsilon^-$ $TCR\beta^-$ $CD19^+$) and monocytes ($Ly6G^-$ $CD3\varepsilon^-$ $TCR\beta^-$ $CD19^-$ $CD11b^+$ $CD115^+$). For mouse spleen, the following $CD45^+$ cell populations were sorted: B cells ($CD19^+$ $MHCII^+$), T cells ($CD3\varepsilon^+$ $TCR\beta^+$ $MHCII^-$), neutrophils ($CD3\varepsilon^-$ $TCR\beta^-$ $CD19^-$ $CD11b^+$ $Ly6G^+$), macrophages ($CD3\varepsilon^-$ $TCR\beta^-$ $CD19^-$ $Ly6G^-$ $F4/80^+$), monocytes ($CD3\varepsilon^-$ $TCR\beta^-$ $CD19^-$ $Ly6G^-$ $F4/80^-$ $CD11b^+$ $CD115^+$) and DCs ($CD3\varepsilon^-$ $TCR\beta^-$ $CD19^-$ $Ly6G^-$ $F4/80^-$ $CD115^-$ $CD11c^+$ $MHCII^+$). For mouse liver, the following $CD45^+$ cell populations were sorted: T cells ($CD3\varepsilon^+$ $TCR\beta^+$ $CD19^-$ $CD20^-$), B cells ($CD19^+$ $CD20^+$ $MHCII^+$) and macrophages ($CD3\varepsilon^-$ $TCR\beta^-$ $CD19^-$ $CD20^-$ $F4/80^+$ $CLEC4F^+$). For mouse lung, the following $CD45^+$ cell populations were sorted: T cells ($CD3\varepsilon^+$ $TCR\beta^+$ $MHCII^-$), neutrophils ($CD3\varepsilon^-$ $TCR\beta^-$ $CD19^-$ $CD11b^+$ $Ly6G^+$), eosinophils ($CD3\varepsilon^-$ $TCR\beta^-$ $CD19^-$ $Ly6G^-$ $CD11b^+$ $SiglecF^+$), alveolar macrophages ($CD3\varepsilon^-$ $TCR\beta^-$ $CD19^-$ $Ly6G^-$ $CD64^+$ $F4/80^+$ $SiglecF^+$ $CD11b^-$), interstitial macrophages ($CD3\varepsilon^-$ $TCR\beta^-$ $CD19^-$ $Ly6G^-$ $CD64^+$ $F4/80^+$ $SiglecF^-$ $CD11b^+$) and DCs ($CD3\varepsilon^-$ $TCR\beta^-$ $CD19^-$ $Ly6G^-$ $CD64^-$ $F4/80^-$ $CD11c^+$ $MHCII^+$). After sorting, cells were centrifuged and lysed in TRIzol reagent or resuspended in the appropriate medium for ex vivo experiments.

For the flow cytometry of mouse AT, samples were acquired on a LSRFortessa X-20 cell analyzer (Becton Dickinson) using the BD FACSDiva Software Version 8.0 (Build 2013 07 02 02 11) (Plateau d'Immunophenotypage Metabolique, Inserm U1011, Lille, France). Analyses were performed with FlowJo software version 10.8 (Becton Dickinson).

Histology

AT (greater omentum in human and epiAT in mice) and liver (needle biopsy of liver in human and full median lobe in mice) were collected and fixed in 4% paraformaldehyde for 48 to 72 h. Tissues were embedded in paraffin by using a STP 120 Spin Tissue Processor (Microm Microtech) and an EG1160 Tissue Embedding Station (Leica). Paraffin-embedded samples were cut at a thickness of 3 μm for liver and 7 μm for AT. Mouse liver tissue sections were transferred on gelatin-coated slides. AT sections were transferred on Superfrost Plus slides (Thermo Scientific cat #J1800AMNZ).

Hematoxylin and eosin (H&E) staining was performed with a Leica autostainer XL set up as followed: xylene (2 min), xylene (2 min), 100% ethanol (2 min), tap water (2 min), hematoxylin (Sigma-Aldrich cat#HHS128) (3 min), tap water (2 min), 70% ethanol 0.25% HCl (6 s), tap water (2 min), 90% ethanol (2 min), eosin (Sigma-Aldrich cat#HT1101128) (2 min), 90% ethanol (6 s), 100% ethanol (1 min) and finished in xylene before covering with a glass coverslip sealed with M-GLAS (Sigma-Aldrich cat#103973).

Immunohistochemistry and immunohistofluorescence were performed after epitope retrieval by using a decloaking chamber NxGen (Bio Care Medical cat#DC2012-220V) (95 °C protocol) with the Diva Decloaker solution (Bio Care Medical cat# DV2004MX). For

immunohistochemistry, tissues were blocked with BLOXALL Endogenous Blocking Solution, Peroxidase and Alkaline Phosphatase (Vector Laboratories cat#SP-6000-100) and serum. Tissues were incubated with monoclonal antibodies against GDF-15 (Novus cat#NBP2-44214) or CD68 (Biolegend cat#916104) overnight at 4 °C in a humidity chamber. Antibody detection was achieved with ImmPRESS® HRP Goat Anti-Rat IgG Polymer Detection Kit, Peroxidase (Vector Laboratories cat#MP-7404), ImmPRESS® HRP Horse Anti-Mouse IgG Polymer Detection Kit, Peroxidase (Vector Laboratories cat#MP-7402) and Vector NovaRED Substrate Kit, Peroxidase (HRP) (Vector Laboratories cat#SK-4800) according to manufacturer's instructions. Tissue sections were counterstained with hematoxylin QS (Vector Laboratories cat#H-3404) and covered with a glass coverslip sealed with M-GLAS (Sigma-Aldrich cat#103973).

For immunohistofluorescence, tissues were blocked with PBS 0.5% BSA 5% donkey serum and co-incubated with monoclonal antibodies against GDF-15 (Novus cat#NBP2-44214) and CD68 (Biolegend cat#916104) overnight at 4 °C in a humidity chamber. Antibody detection was achieved with AF647 AffiniPure Donkey Anti-Rat IgG (Jackson ImmunoResearch cat#712-605-153) and AF488 AffiniPure Donkey Anti-Mouse IgG (Jackson ImmunoResearch cat#715-545-151). Tissue sections were counterstained with NucBlue Fixed Cell ReadyProbes Reagent (DAPI) (Invitrogen cat#R37606) and mounted with Dako Fluorescence Mounting Medium (Agilent cat#S3023).

H&E- and immunohistochemistry-stained slides were acquired on an Eclipse Ti-U inverted microscope (Nikon) using the NIS-Elements BR Imaging software version 4.20.03 (Build 995) 64 bit. Acquisition of immunohistofluorescence images was performed on a LSM 880 confocal microscope (Zeiss). Images were prepared with Image J software version 1.53t (NIH, https://imagej.nih.gov/ij/).

Transcriptomic analysis

Microarrays of liver biopsies from the ABOS cohort were normalized by the robust multi-average method using oligo/Bioconductor. Multiple probes mapped to a single gene were collapse by using the mean of expression. Log_2 expression values were used for analyses. Raw data were previously made available at GEO under the accession number GSE130991[58].

Microarrays of human monocytes and MDM were analyzed with GEO2R and default settings (https://www.ncbi.nlm.nih.gov/geo/geo2r/). Raw data are available at GEO under the accession number GSE5099[66].

RNA-sequencing data of mouse immune cell populations were assembled by the Immunological Genome Project[67] (ImmGen, http://www.immgen.org/) and accessed through the ImmGen open access web portal (http://rstats.immgen.org/Skyline/skyline.html) (Data set used: ImmGen ULI RNA-seq). Raw data are available at GEO under the accession number GSE127267.

Single-cell RNA-sequencing (scRNA-seq)

scRNA-seq were performed on $CD45^+$ sorted cells from epiAT of C57BL/6 J mice on 10% LFD or 60% HFD for 27 weeks[31]. Raw data are available at GEO under the accession number GSE182233. *Gdf15* expression was visualized from the open access web portal provided by authors (https://hastylab.shinyapps.io/MAIseq/) without any further modifications. Cluster annotations were collected from the original publication[31] and have not been modified. The proper identification of macrophage cluster was confirmed by verifying the expression of specific macrophage markers.

Gene set enrichment analysis (GSEA)

GSEA analyses were performed with GSEA[68] version 4.3.2 (https://www.gsea-msigdb.org/gsea/index.jsp) on the liver transcriptomic data. The following human gene sets were used: TFEB_TARGET_GENES (M30207), EGR1_01 (M1532), CHOP_01 (M9852) and the GO:BP (GO biological process, 7751 gene sets, c5.go.bp.v2022.1.Hs.symbols.gmt). The following parameters were selected: number of permutations, 1000; permutation type, phenotype; collapse/remap to gene symbols, collapse; max size, 2000; min size, 5.

Statistical analyses

All statistical analyses were carried out using GraphPad Prism 9 for Windows (GraphPad Software) and presented as means ± standard error of the mean (SEM). Data were analyzed with the following non-parametric tests: Mann–Whitney test, Kruskal–Wallis test followed by Dunn's multiple comparisons test, Wilcoxon matched-pairs signed rank test, Friedman test followed by Dunn's multiple comparisons test and Spearman correlation. When multiple Mann–Whitney tests were used, a false discovery rate correction was applied by using the two-stage step-up method of Benjamini, Krieger and Yekutieli. Non-parametric tests were mainly used because *GDF15* expression and plasma GDF-15 concentration were non-normally distributed in our cohort, as assessed by Shapiro–Wilk normality test, and the sample sized for in vitro and mice experiments were too small to always guarantee data normality. To examine the influence of two independent variables, 2-way ANOVA followed by Sidak's, Holm–Sidak's or Dunnett's multiple comparisons test was used. All statistical tests were two-tailed.

Simple and multiple linear regressions were performed using R open source software (version 4.3.1) and gtsummary package. Receiver operating characteristic (ROC) curve analysis was performed with Wilson/Brown method for confidence interval calculation. ROC curves were calculated according to *GDF15* mRNA expression levels in liver measured by microarray in 840 patients with obesity. Binary classifications from these 840 patients were the following: MASL ($n = 623$ MASL vs 139 no MASLD), MASH ($n = 78$ MASH vs 139 no MASLD & 623 MASL), steatosis ($n = 701$ steatosis ≥ 1 vs 139 steatosis = 0), inflammation ($n = 258$ inflammation ≥ 1 vs 582 inflammation = 0) and ballooning ($n = 110$ ballooning ≥ 1 vs 730 ballooning = 0).

All statistics details including statistical test used, exact value of n and statistical significance are reported in figure legend. Alpha level was set at 0.05. Each data point represents genuine replication (biological replicates) and was obtained from a single measurement or from multiple measurements illustrated by the mean.

Reporting summary

Further information on research design is available in the Nature Portfolio Reporting Summary linked to this article.

Data availability

No new datasets were generated during the current study. Access to individual data is restricted to protect the privacy of study participants and to comply with ethical and legal requirements governing the use of health-related data. The data can only be accessed under specific conditions which include signing a data use agreement that ensures the data will be used solely for the intended research purposes. To gain access to the data, researchers must submit a detailed request outlining their research objectives and methodology. Requests for data access should be directed to the principal investigator of ABOS study cohort Dr. François Pattou (Francois.pattou@univ-lille.fr). The data will be made available only to researchers affiliated with recognized institutions and for the purpose of conducting research that aligns with the original scope and objectives of the ABOS cohort study. We aim to respond to access requests within 30 days. This timeframe may vary depending on the volume of requests and the completeness of the submitted documentation. Once access has been granted, the data will be available to the requesting researcher for a period of one year. Extensions may be granted upon request and subject to review. The transcriptomic data used in this study are available in the GEO database under accession codes GSE130991, GSE5099, GSE127267 and GSE182233. The authors declare that the main data supporting the

findings of this study are available within the paper and its supplementary information file. Source data are provided with this paper.

References

1. Chavakis, T., Alexaki, V. I. & Ferrante, A. W. Macrophage function in adipose tissue homeostasis and metabolic inflammation. *Nat. Immunol.* **24**, 757–766 (2023).
2. McNelis, J. C. & Olefsky, J. M. Macrophages, immunity, and metabolic disease. *Immunity* **41**, 36–48 (2014).
3. Azzu, V., Vacca, M., Virtue, S., Allison, M. & Vidal-Puig, A. Adipose tissue-liver cross talk in the control of whole-body metabolism: implications in nonalcoholic fatty liver disease. *Gastroenterology* **158**, 1899–1912 (2020).
4. Geng, Y., Faber, K. N., de Meijer, V. E., Blokzijl, H. & Moshage, H. How does hepatic lipid accumulation lead to lipotoxicity in non-alcoholic fatty liver disease? *Hepatol. Int.* **15**, 21–35 (2021).
5. Fairlie, W. D. et al. MIC-1 is a novel TGF-beta superfamily cytokine associated with macrophage activation. *J. Leukoc. Biol.* **65**, 2–5 (1999).
6. Paralkar, V. M. et al. Cloning and characterization of a novel member of the transforming growth factor-beta/bone morphogenetic protein family. *J. Biol. Chem.* **273**, 13760–13767 (1998).
7. Ding, Q. et al. Identification of macrophage inhibitory cytokine-1 in adipose tissue and its secretion as an adipokine by human adipocytes. *Endocrinology* **150**, 1688–1696 (2009).
8. Hsu, J.-Y. et al. Non-homeostatic body weight regulation through a brainstem-restricted receptor for GDF15. *Nature* **550**, 255–259 (2017).
9. Mullican, S. E. et al. GFRAL is the receptor for GDF15 and the ligand promotes weight loss in mice and nonhuman primates. *Nat. Med.* **23**, 1150–1157 (2017).
10. Yang, L. et al. GFRAL is the receptor for GDF15 and is required for the anti-obesity effects of the ligand. *Nat. Med.* **23**, 1158–1166 (2017).
11. Wang, D. et al. GDF15 promotes weight loss by enhancing energy expenditure in muscle. *Nature* **619**, 143–150 (2023).
12. Tsai, V. W. W., Husaini, Y., Sainsbury, A., Brown, D. A. & Breit, S. N. The MIC-1/GDF15-GFRAL pathway in energy homeostasis: implications for obesity, cachexia, and other associated diseases. *Cell Metab* **28**, 353–368 (2018).
13. Chrysovergis, K. et al. NAG-1/GDF-15 prevents obesity by increasing thermogenesis, lipolysis and oxidative metabolism. *Int. J. Obes. 2005* **38**, 1555–1564 (2014).
14. Chung, H. K. et al. Growth differentiation factor 15 is a myomitokine governing systemic energy homeostasis. *J. Cell Biol.* **216**, 149–165 (2017).
15. Bootcov, M. R. et al. MIC-1, a novel macrophage inhibitory cytokine, is a divergent member of the TGF-beta superfamily. *Proc. Natl. Acad. Sci. USA* **94**, 11514–11519 (1997).
16. Govaere, O. et al. Transcriptomic profiling across the nonalcoholic fatty liver disease spectrum reveals gene signatures for steatohepatitis and fibrosis. *Sci. Transl. Med.* **12**, eaba4448 (2020).
17. Patel, S. et al. Combined genetic deletion of GDF15 and FGF21 has modest effects on body weight, hepatic steatosis and insulin resistance in high fat fed mice. *Mol. Metab.* **65**, 101589 (2022).
18. Tran, T., Yang, J., Gardner, J. & Xiong, Y. GDF15 deficiency promotes high fat diet-induced obesity in mice. *PloS One* **13**, e0201584 (2018).
19. Li, D., Zhang, H. & Zhong, Y. Hepatic GDF15 is regulated by CHOP of the unfolded protein response and alleviates NAFLD progression in obese mice. *Biochem. Biophys. Res. Commun.* **498**, 388–394 (2018).
20. Macia, L. et al. Macrophage inhibitory cytokine 1 (MIC-1/GDF15) decreases food intake, body weight and improves glucose tolerance in mice on normal & obesogenic diets. *PloS One* **7**, e34868 (2012).
21. Dostálová, I. et al. Increased serum concentrations of macrophage inhibitory cytokine-1 in patients with obesity and type 2 diabetes mellitus: the influence of very low calorie diet. *Eur. J. Endocrinol. Eur. Fed. Endocr. Soc.* **161**, 397–404 (2009).
22. Kempf, T. et al. Growth differentiation factor 15 predicts future insulin resistance and impaired glucose control in obese non-diabetic individuals: results from the XENDOS trial. *Eur. J. Endocrinol.* **167**, 671–678 (2012).
23. Koo, B. K. et al. Growth differentiation factor 15 predicts advanced fibrosis in biopsy-proven non-alcoholic fatty liver disease. *Liver Int. Off. J. Int. Assoc. Study Liver* **38**, 695–705 (2018).
24. Vila, G. et al. The relationship between insulin resistance and the cardiovascular biomarker growth differentiation factor-15 in obese patients. *Clin. Chem.* **57**, 309–316 (2011).
25. Kim, J. et al. TFEB-GDF15 axis protects against obesity and insulin resistance as a lysosomal stress response. *Nat. Metab.* **3**, 410–427 (2021).
26. Patel, S. et al. GDF15 provides an endocrine signal of nutritional stress in mice and humans. *Cell Metab* **29**, 707–718.e8 (2019).
27. Chen, X., Tang, Y., Chen, S., Ling, W. & Wang, Q. IGFBP-2 as a biomarker in NAFLD improves hepatic steatosis: an integrated bioinformatics and experimental study. *Endocr. Connect.* **10**, 1315–1325 (2021).
28. L'homme, L. et al. Deletion of the nuclear receptor RORα in macrophages does not modify the development of obesity, insulin resistance and NASH. *Sci. Rep.* **10**, 21095 (2020).
29. Cinti, S. et al. Adipocyte death defines macrophage localization and function in adipose tissue of obese mice and humans. *J. Lipid Res.* **46**, 2347–2355 (2005).
30. Lumeng, C. N., Bodzin, J. L. & Saltiel, A. R. Obesity induces a phenotypic switch in adipose tissue macrophage polarization. *J. Clin. Invest.* **117**, 175–184 (2007).
31. Cottam, M. A., Caslin, H. L., Winn, N. C. & Hasty, A. H. Multiomics reveals persistence of obesity-associated immune cell phenotypes in adipose tissue during weight loss and weight regain in mice. *Nat. Commun.* **13**, 2950 (2022).
32. Barreby, E., Sulen, A. & Aouadi, M. Glucan-encapsulated siRNA particles (GeRPs) for specific gene silencing in adipose tissue macrophages. *Methods Mol. Biol. Clifton NJ* **1951**, 49–57 (2019).
33. Emmerson, P. J. et al. The metabolic effects of GDF15 are mediated by the orphan receptor GFRAL. *Nat. Med.* **23**, 1215–1219 (2017).
34. Wrobel, L., Siddiqi, F. H. & Rubinsztein, D. C. Transient siRNA-mediated protein knockdown in mouse followed by feeding/starving cycle and liver tissue analysis. *STAR Protoc.* **2**, 100500 (2021).
35. Tan, A., Prasad, R., Lee, C. & Jho, E.-H. Past, present, and future perspectives of transcription factor EB (TFEB): mechanisms of regulation and association with disease. *Cell Death Differ* **29**, 1433–1449 (2022).
36. Xie, Y., Li, Y., Chen, J., Ding, H. & Zhang, X. Early growth response-1: key mediators of cell death and novel targets for cardiovascular disease therapy. *Front. Cardiovasc. Med.* **10**, 1162662 (2023).
37. Yang, Y. et al. Transcription factor C/EBP homologous protein in health and diseases. *Front. Immunol.* **8**, 1612 (2017).
38. Osman, A. et al. Identification of genomic binding sites and direct target genes for the transcription factor DDIT3/CHOP. *Exp. Cell Res.* **422**, 113418 (2023).
39. Haas, J. T. et al. Transcriptional network analysis implicates altered hepatic immune function in NASH development and resolution. *Nat. Metab.* **1**, 604–614 (2019).
40. Hsiao, E. C. et al. Characterization of growth-differentiation factor 15, a transforming growth factor beta superfamily member induced following liver injury. *Mol. Cell. Biol.* **20**, 3742–3751 (2000).
41. Jiang, P. et al. Growth differentiation factor 15 is dispensable for acetaminophen-induced liver injury in mice. *Basic Clin. Pharmacol. Toxicol.* **132**, 343–353 (2023).
42. Dubois, V. et al. Endoplasmic reticulum stress actively suppresses hepatic molecular identity in damaged liver. *Mol. Syst. Biol.* **16**, e9156 (2020).

43. Tsuchiya, M. et al. Interstrain differences in liver injury and one-carbon metabolism in alcohol-fed mice. *Hepatol. Baltim. Md* **56**, 130–139 (2012).
44. Tian, R.-D. et al. Phosphorylation of eIF2α mitigates endoplasmic reticulum stress and hepatocyte necroptosis in acute liver injury. *Ann. Hepatol.* **19**, 79–87 (2020).
45. Ben Mosbah, I. et al. Endoplasmic reticulum stress inhibition protects steatotic and non-steatotic livers in partial hepatectomy under ischemia-reperfusion. *Cell Death Dis.* **1**, e52 (2010).
46. Uzi, D. et al. CHOP is a critical regulator of acetaminophen-induced hepatotoxicity. *J. Hepatol.* **59**, 495–503 (2013).
47. Lian, Y.-E., Bai, Y.-N., Lai, J.-L. & Huang, A.-M. Aberrant regulation of autophagy disturbs fibrotic liver regeneration after partial hepatectomy. *Front. Cell Dev. Biol.* **10**, 1030338 (2022).
48. Samuvel, D. J. et al. Mitochondrial depolarization after acute ethanol treatment drives mitophagy in living mice. *Autophagy* **18**, 2671–2685 (2022).
49. Bao, X. et al. Growth differentiation factor 15 is positively associated with incidence of diabetes mellitus: the Malmö Diet and Cancer-Cardiovascular Cohort. *Diabetologia* **62**, 78–86 (2019).
50. Brown, D. A. et al. MIC-1 serum level and genotype: associations with progress and prognosis of colorectal carcinoma. *Clin. Cancer Res. Off. J. Am. Assoc. Cancer Res.* **9**, 2642–2650 (2003).
51. Brown, D. A. et al. Concentration in plasma of macrophage inhibitory cytokine-1 and risk of cardiovascular events in women: a nested case-control study. *Lancet Lond. Engl.* **359**, 2159–2163 (2002).
52. Benichou, O. et al. Discovery, development, and clinical proof of mechanism of LY3463251, a long-acting GDF15 receptor agonist. *Cell Metab* **35**, 274–286.e10 (2023).
53. Zhang, Y. et al. Activity-balanced GLP-1/GDF15 dual agonist reduces body weight and metabolic disorder in mice and non-human primates. *Cell Metab* **35**, 287–298.e4 (2023).
54. Wang, C. et al. Small-molecule TFEB pathway agonists that ameliorate metabolic syndrome in mice and extend C. elegans lifespan. *Nat. Commun.* **8**, 2270 (2017).
55. Caiazzo, R. et al. Roux-en-Y gastric bypass versus adjustable gastric banding to reduce nonalcoholic fatty liver disease: a 5-year controlled longitudinal study. *Ann. Surg.* **260**, 893–898 (2014).
56. Raverdy, V. et al. Data-driven subgroups of type 2 diabetes, metabolic response, and renal risk profile after bariatric surgery: a retrospective cohort study. *Lancet Diabetes Endocrinol.* **10**, 167–176 (2022).
57. Kleiner, D. E. et al. Design and validation of a histological scoring system for nonalcoholic fatty liver disease. *Hepatol. Baltim. Md* **41**, 1313–1321 (2005).
58. Margerie, D. et al. Hepatic transcriptomic signatures of statin treatment are associated with impaired glucose homeostasis in severely obese patients. *BMC Med. Genomics* **12**, 80 (2019).
59. American Diabetes Association. Diagnosis and classification of diabetes mellitus. *Diabetes Care* **37**, S81–S90 (2014).
60. Rinella, M. E. et al. A multi-society Delphi consensus statement on new fatty liver disease nomenclature. *J. Hepatol.* S0168-8278(23)00418-X https://doi.org/10.1016/j.jhep.2023.06.003 (2023).
61. Esser, N. et al. Obesity phenotype is related to NLRP3 inflammasome activity and immunological profile of visceral adipose tissue. *Diabetologia* **56**, 2487–2497 (2013).
62. Cheval, L. et al. Acidosis-induced activation of distal nephron principal cells triggers Gdf15 secretion and adaptive proliferation of intercalated cells. *Acta Physiol. Oxf. Engl.* **232**, e13661 (2021).
63. L'homme, L. et al. Unsaturated fatty acids prevent activation of NLRP3 inflammasome in human monocytes/macrophages. *J. Lipid Res.* **54**, 2998–3008 (2013).
64. Schippers, I. J. et al. Immortalized human hepatocytes as a tool for the study of hepatocytic (de-)differentiation. *Cell Biol. Toxicol.* **13**, 375–386 (1997).
65. de Jonge, H. J. M. et al. Evidence based selection of housekeeping genes. *PLoS One* **2**, e898 (2007).
66. Martinez, F. O., Gordon, S., Locati, M. & Mantovani, A. Transcriptional profiling of the human monocyte-to-macrophage differentiation and polarization: new molecules and patterns of gene expression. *J. Immunol. Baltim. Md 1950* **177**, 7303–7311 (2006).
67. Heng, T. S. P., Painter, M. W. & Immunological Genome Project Consortium. The Immunological Genome Project: networks of gene expression in immune cells. *Nat. Immunol.* **9**, 1091–1094 (2008).
68. Subramanian, A. et al. Gene set enrichment analysis: a knowledge-based approach for interpreting genome-wide expression profiles. *Proc. Natl. Acad. Sci. USA* **102**, 15545–15550 (2005).

Acknowledgements

This research has been funded by grants from the "European Genomic Institute for Diabetes" and ANR (E.G.I.D., ANR-10-LABX-46 to B.S. and F.P., ANR-18-CE15-0024-03_ACT to B.S. and D.D., and ANR-20-CE14-0034 to D.D.). This work was also supported by the "Program d'Investissement d'Avenir" (PRECINASH, ANR-16-RHUS-0006 to F.P. and B.S.), Lille University (WILL-CHAlRES-23-001 to F.P.), Fondation de la Recherche Médicale (EQU202303016330 PATTOU to F.P.), EU Horizon 2020 research and innovation program (Innovative Medicines Initiative 2, project SOPHIA 875534 to F.P.). N.E. is a F.R.S-FNRS Post-Doctorate Clinical Master Specialist. J.T.H. is supported by an ERC-Starting Grant (Metabo3DC, contract number: 101042759). The authors thank the BioImaging Center Lille (BICeL, France) and the Plateau d'Immunophenotypage Metabolique (U1011-EGID, Lille, France) for cell sorting and microscopy. The authors are grateful to Viviane Gnemmi, Emmanuelle Leteurtre, Guillaume Lassailly, Philippe Mathurin for their invaluable contribution to liver phenotype characterization of ABOS cohort participants. The authors also thank Benoit Pourcet (U1011-EGID, Lille, France) for his help for the confocal microscopy, Bruno Derudas (U1011-EGID, Lille, France) for his technical assistance and Jérome Noulette (deceased) for data and sample management.

Author contributions

Conceptualization, L.L., B.S. and D.D.; methodology, L.L., J.T.H., M.A., F.P., B.S. and D.D.; investigation, L.L., B.P.S., J.T.H., S.F., S.Q., V.G. and N.E.; formal analysis, L.L.; validation, L.L. and D.D.; resources, L.L., B.P.S., J.T.H., E.B., N.E., R.C., H.V., V.R., B.L., L.C., N.P., J.P., S.L-P., M.A., F.P. and D.D.; writing—original draft preparation, L.L., B.S. and D.D.; supervision, B.S. and D.D.; funding acquisition, B.S. and D.D.. All authors have read and agreed to the published version of the manuscript.

Competing interests

The authors declare no competing interests.

Additional information

Supplementary information The online version contains supplementary material available at https://doi.org/10.1038/s41467-024-51078-2.

Correspondence and requests for materials should be addressed to Laurent L'homme or David Dombrowicz.

Peer review information *Nature Communications* thanks Dongdong Wang and the other anonymous reviewer(s) for their contribution to the peer review of this work. A peer review file is available.